Optimising the propeller hull interaction of a parametric aft ship using optimisation algorithms

V.J.J. Elderhorst

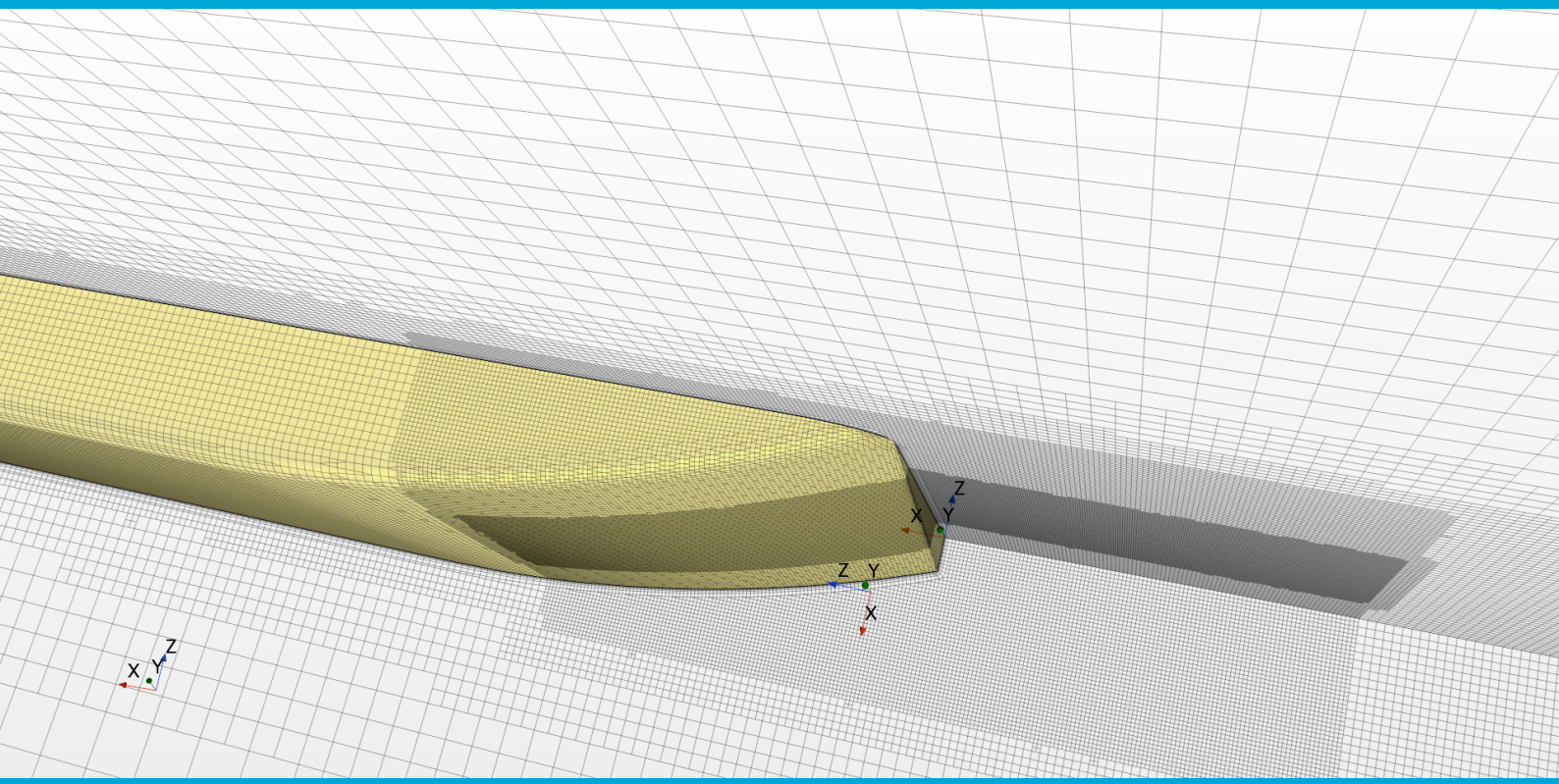

TU Delft

VUYK ENGINEERING

Optimising the propeller hull interaction of a parametric aft ship using optimisation algorithms

by

V.J.J. Elderhorst

to obtain the degree of Master of Science
at the Delft University of Technology,

Student number:	4731573	
Project duration:	October 3, 2023 – September 5, 2024	
Thesis supervisors:	Prof. dr. ir. T. van Terwisga,	TU Delft, supervisor
	Ir. R. de Vries,	Vuyk engineering
	Ir. M. Garenaux,	Marin
Graduation committee:	Prof. dr. ir. T. van Terwisga,	TU Delft, supervisor
	Ir. R. de Vries,	Vuyk engineering
	Ir. M. Garenaux,	Marin
	Dr. D. Fiscaletti,	TU Delft
	Dr. A. Coraddu,	TU Delft

TU Delft

VUYK ENGINEERING

Contents

Abstract

V.J.J. Elderhorst

The ongoing pursuit of efficiency in the shipping industry is driven by both economic and environmental objectives. While historically focused on reducing fuel consumption to enhance market competitiveness, recent regulations such as the International Maritime Organisation's Energy Efficiency Design Index (EEDI) and Energy Efficiency Existing Index (EEXI) have emphasized the need to minimize harmful emissions. To achieve these goals, Simulation-Based Design (SBD) and Computational Fluid Dynamics (CFD) have become essential tools for optimizing ship design. This research aims to develop and implement an optimization strategy to minimize the propeller power required for a vessel to maintain a constant speed by refining the aftbody shape while accounting for propeller-hull interaction effects.

The study addresses a critical gap in current methodologies, where many existing optimization strategies neglect propeller effects and studies including propeller effects use too computationally intensive methods to be used in an optimisation strategy. The research explores strategies to reduce computational load, ensuring a balance between accuracy and efficiency. Key questions include determining the optimal geometrical parameters for aftbody design, refining CFD procedures to be computationally light yet accurate, incorporating propeller effects efficiently, and identifying the most effective optimization algorithm.

The research findings reveal that by varying specific geometrical parameters, such as the aft arc angle and transom angle, an approximately 10% reduction in required propeller power can be achieved. The study also evaluates different strategies for reducing computational load, including a grid refinement study and the exclusion of free surface effects, while noting the trade-offs in accuracy. The use of the virtual disk method to model propeller effects is identified as the most practical approach given computational constraints. Among the optimization algorithms tested, the NSGA-III algorithm is found to be the most effective, offering significant improvements with fewer computational resources compared to alternatives.

Overall, the research demonstrates that the proposed optimization setup can lead to a significant reduction in propeller power, contributing to the development of more efficient ship designs. However, further research is needed to refine the exclusion and estimation of free surface effects to ensure broader applicability across different vessel designs.

I

Theory

1 Introduction

In the shipping industry, there is an endless drive for efficiency. This has always had a financial goal, a more efficient ship with lower fuel usage allows for a more competitive position in the market. More recently however there is also an environmental goal for improving efficiency in shipping since a more efficient vessel will emit less harmful emissions into the atmosphere. This second goal is exemplified by the Energy Efficiency Design Index (EEDI) and Energy Efficiency Existing Index (EEXI) of the International Maritime Organisation (IMO). One of the tools to improve efficiency, especially in new designs is Simulation-Based Design (SBD), where continuous improvements in computing power allows for more detailed evaluation of the design properties in earlier stages of the design process. The hydrodynamic properties in these designs can be evaluated using Computational Fluid Dynamics (CFD) which also greatly benefits from the same increase in computing power. In this research project, SBD will be used to optimise the shape of the aftbody of a vessel while also taking the propeller-hull interaction effects into account. The optimisation will be done using an optimisation algorithm.
Although progress has been made concerning computing power, the resources of every organisation including Vuyk Engineering are not limitless. Because of this computing power and time are two limiting factors when making use of computer design. For this reason, great effort will be put into minimising the computational resources and the time needed to execute this research project.

1.1. Problem statement

Multiple papers have been found discussing using an optimisation algorithm to optimise the hull shape of a vessel [16], some are focused on optimising the bulb shape[33] [34]. Most of the papers analysed describe research into optimising the aft of the hull [27] [28] [17] [20] [18]. Most of the analysed papers simulate a ship without a propeller and the ones that do, make use of computationally intensive methods. If an optimisation strategy only focuses on reducing the resistance, the propeller efficiency might be reduced because of a less efficient flow around the propeller. This might lead to increased required propeller power, leading to increased fuel consumption. Because of this incorporating the propeller in the analysis can be beneficial for the optimisation results. It is however also not feasible for most designers in the maritime industry to optimise a hull while modelling the propeller with a Reynolds Averaged Navier Stokes (RANS) model. Because of these reasons, there is a demand for an optimisation method that incorporates the propeller-hull interaction effects, but is also relatively computationally light.

1.2. Research goal

The goal of this research is to develop and execute an optimisation strategy which is able to optimise the shape of the aftbody of a vessel to minimise the propeller power required for a vessel to sail at a constant speed. From this goal, the following research questions can be formed:

- What geometrical parameters will need to be adjustable to be able to design the optimum aft shape?

- How can a CFD procedure be computationally light enough for an optimisation study using currently known techniques, while still being accurate and with enough resolution?
- How can the effects of a propeller be incorporated in an accurate way and with enough resolution into the CFD analysis while not adding as much computational load to make it unsuitable for an optimisation study?
- Which currently known optimisation method is the most effective and most efficient for this type of optimisation study?

2

Plan of Approach

This chapter will explain the plan of approach which will be followed to answer the previously stated research questions.

2.1. Base vessel

An optimisation strategy can be greatly simplified with the right starting point and the right limits. To aid in this, the type of vessel which will be the subject of this research project will need to be investigated. The base vessel will be a heavy transport vessel which will be propelled by twin ducted propulsor pods. The objective of this vessel is to transport large converter stations from their port of construction, mostly in Asia, to windfarm projects all over the world. This vessel has two main sailing conditions, one while sailing fully loaded and one while sailing in ballast condition. One condition must be chosen as the optimisation goal due to computational limits and because there is a significant difference in the power requirements. One of the main reasons for this difference in power requirements is the wind area of these converter stations, the details about the total air resistance will be discussed in paragraph 2.4.3. Because of this, the choice is made to optimise for the design condition, which is the fully loaded condition. According to the operational profile, the vessel will be sailing the majority of the time under this condition.

2.2. Designing the model

The 3D model of the hull will be designed using Rhinoceros and the plug-in grasshopper. RhinoCeros is a 3D modelling tool which is widely used in the shipbuilding industry. Grasshopper is a visual programming language for Rhinoceros which can be used to build a parametric model. For a model to be used in an optimisation study the model needs to be parametric, these parameters will all have geometric significance. This allows the possibility of relating the result to specific geometric properties of the hull. The propellers of the pod itself will be modelled using an Actuator Disk while the strut of the pod will not be modelled. This is because of the assumption that the base will not have a significant effect on the total resistance and that the struts will not have a big effect on the flow around the aft of the vessel and thus not have a big effect on the optimisation.

2.3. Optimisation goal

As stated in the research goal, the optimisation goal is to minimise the required propeller power. This optimisation goal is chosen for multiple reasons. First, the propeller power relates more directly to fuel consumption than for example ship resistance or thrust would. Thus reducing the propeller power is more effective in designing more efficient ships. Propeller power also does not require the estimating of a shaft or gearbox efficiency which falls outside the scope of this research. Another advantage of propeller power is that it incorporates all the propeller hull effects in contrast to thrust, by also incorporating the wake fraction. How the propeller power can be determined will be discussed in chapter 3.

2.4. CFD analysis

The fluid dynamic properties of the different iterations of this parameterised model will be calculated using the software package STAR-CCM+. These calculations will need to be as computationally light as possible. This is because the optimisation process will need to calculate many iterations to be able to achieve significant results and to be able to incorporate as many parameters as possible. To achieve this only half of the hull in the longitudinal direction will be modelled, with the assumption that the flow will be symmetrical at the longitudinal symmetry plan. This assumption is deemed valid because of the twin-pod design of the base vessel which makes the vessel symmetrical. Also, the timestep and grid size will be as large as can be achieved without significantly reducing the accuracy and resolution. How this can be achieved will be discussed in chapter 3. The last possibility which will be researched to save computing power is to calculate only the aft part of the model. Since this process has not been widely discussed in other papers yet, the technique and justification will be discussed in the next paragraph.

2.4.1. Partial CFD analysis

To save computational time only the aft of the different iterations of the hull model will be analysed. Since there is little literature about this subject the validity needs to be determined first. This will be done by first analysing the whole model and using the flow around the front part as the boundary criteria for the inflow while analysing the aft part of the same iteration of the model. Next, the flows, pressure and predicted power from both analyses will be compared to test if only analysing the aft part of the model will give an accurate representation. When this is the case this method will be used for all the other iterations.

2.4.2. Free surface and trim effects

When the above-mentioned technique is implemented free surface effects such as waves cannot be modelled. Because of this, the assumption will need to be made that the changes to the aftbody of the ship will not have a significant effect on the wave-making resistance. Although this assumption has also been implemented in previous research [17], great care needs to be taken to make sure that this assumption is justified. This reasoning also applies to the trim and sinkage effects

2.4.3. Air resistance

A preliminary resistance overview made by Vuyk Engineering estimates that the wind resistance can be between 20% and 25% of the total resistance, because of the large frontal area of the transformation stations. Because of this, the effect of air resistance will need to be incorporated into the CFD calculations. This will use a similar method to the previously mentioned method to incorporate the resistance of the front part of the model. The air resistance will be estimated for the design speed and incorporated into the total resistance of the vessel. This will allow for an accurate estimation of the required thrust and thus the propeller power.

2.4.4. Propulsion

The pod propulsion will be modelled using an Actuator Disk model. The actuator disk model uses the total resistance to determine the propeller properties. Because of this, the total resistance will be modelled by adding the resistance from the analysis of the aft, the analysis from the front originating from the analysis of the full hull, the air resistance caused by the frontal area of the converter station and an estimation of the wave making resistance. To validate this method this resistance will be compared with the resistance from the full hull analysis. The propeller itself will be chosen from the Wageningen Ka series and optimised for both propeller speed and P/D while keeping the propeller diameter constant based on the initial design. Previous experience teaches that the P/D ratio for the propeller can also be assumed constant throughout the optimisation process. Because of this, only a single open water curve will need to be analysed for every variation in the design.

2.5. Optimisation

With the CFD calculations working, an optimisation framework needs to be set up. Also, an optimisation strategy will need to be chosen.

2.5.1. Workflow

To be able to build this optimisation framework first the current workflow needs to be illustrated. This is done in figure 2.1. As can be seen, the workflow starts with creating a list of desired values for the

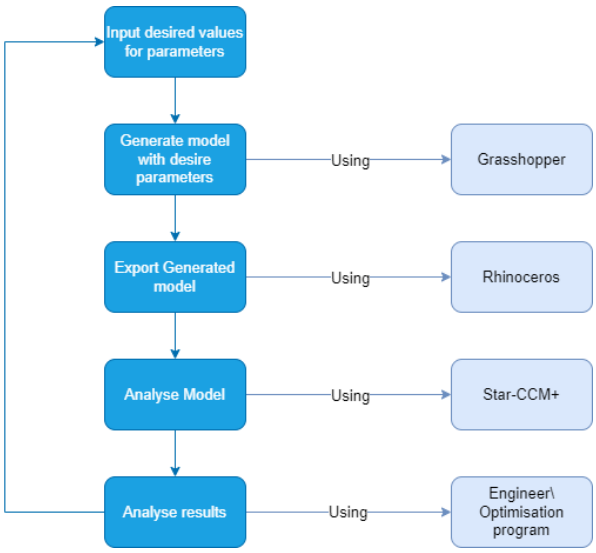

Figure 2.1: Schematic of the workflow

changeable parameters within the limited design space which has been examined beforehand. In the classical design approach, these values will be determined by a designer based on previous experience and sometimes previous design iterations or other similar projects. An optimisation strategy can only determine these values based on previous iterations or a certain distribution criterion to create a list of starting designs.
Next the model itself will need to be designed based on these values. This will be done using the program Grasshopper which is a visual programming language for the 3D modelling software Rhinoceros. The Grasshopper file is used to create a fully parametric design with a limited design space. This limited design space prevents the generation of unfeasible designs.
After the design is generated in Grasshopper, Rhinoceros will be used to create a model which can be used for the CFD analysis. With the set-up of the previously mentioned Grasshopper model, care needs to be given to the fact that the resulting model will be usable in the set framework for the CFD analysis.
Star-CCM+ will then be used to perform the CFD analysis. Again similar to the Grasshopper model care needs to be given while designing the framework for this analysis, to make sure that all generated designs can be evaluated.
Finally, the results from the CFD analysis need to be analysed. Just as with determining the starting values there is a difference in how a designer will analyse these results and how an optimisation program will do that. A designer will analyse the results using previous experience and while looking at a broad amount of parameters. An optimisation strategy can only analyse the parameters for which it is designed, also if more parameters need to be taken into account more variations on the model need to be analysed.

2.5.2. Automating the workflow

As can be seen in the above section to be able to develop an optimisation strategy the workflow needs to be automated and developed in such a way that no issue can occur which the optimisation strategy can not handle. To achieve this the program HEEDS by Siemens will be used to execute the optimisation and manage the workflow. HEEDS makes use of Python scripts to be able to communicate with the other required programs in the workflow. HEEDS will make use of an optimisation algorithm to analyse the results of previous variations and determine the values for the parameters for the new iterations of designs. The specifics of optimisation algorithms are described in chapter 3.

2.6. Performing the study

Before the definite study is performed first a test study will be run. This is a study which evaluates a limited amount of designs intending to catch any previously unnoticed bugs. This test study can also be used to estimate if the chosen optimisation algorithm can be expected to determine an improved result using the given amount of designs. If this test study is successful a definite study will be performed. However, if the test study reveals unexpected results adjustments will be made to the study and a second test study will be run.

2.7. Uncertainty analysis

When analysing the results, the errors and uncertainties also need to be analysed. Another chapter will go more into detail about the different types of errors. The analysis itself will be performed according to the ITTC guidelines [14].

3

Literature research

One of the first steps in conducting scientific research is performing a literature study. This is done to achieve the following goals: give an overview of the most up-to-date research being performed related to the field; seeing if the proposed research is a unique proposal which will add to the field and get an overview of the theoretical background necessary to achieve the proposed research goal.

3.1. Overview of current research

Three related fields of study are researched in this literature study. The first field is the use of CFD while optimising the hull shape, most of the reviewed research focuses on the aft of the ship, but research focusing on the bulb or the complete hull has also been evaluated. Another field is the modelling of the propeller hull interactions, most of the time analysed with CFD methods. The final field is the optimisation methods themselves.

3.1.1. CFD analyses methods

This section attempts to review which CFD methods are used when optimising the hull shape of a vessel. The most used method is the Reynolds Averaged Navier Stokes (RANS) method [33] [16] [34] [27] [28] [18]. The advantages of this method are that it is relatively computationally light for less complex shapes like a ship hull and gives accurate estimations while being capable of modelling viscous effects in the flow. The classic RANS model however needs turbulence models to be able to incorporate turbulence in the overall analysis. The two most frequently used turbulence models in RANS simulations are the k-ϵ and k-ω models. These two however both have their issues, one notable being that the k-ϵ model contains terms which are undefined at the wall [11]. This is commonly solved using wall functions. The k-ω model can more accurately model the flow along the wall, but is very sensitive to the free stream value of ω, thus increasing the sensitivity further away from the wall [11]. One solution for this is the Shear Stress Transport (SST) model, which allows for the use of the k-ω model near and at the walls and transitions to the k-ϵ further away from the wall. This allows for a fully resolved flow up to the wall without the increased sensitivity further away from the wall. This makes the SST model suitable for flows which resolve fully up to the wall.
Two other commonly used methods for modelling the flow around a ship are the Boundary Element Method (BEM) and the Large Eddy Simulation (LES) method or its Detached Eddy Simulations (DES) variant. BEM is based on potential flow theory. It divides the flow domain into bounding panels and solves the non-vicious flowfield by solving the Laplace equations for the boundary conditions on those panels. Because of this BEM is a different flow model than RANS and LES. Although BEM is computationally less intensive than RANS, BEM also does not model viscous effects directly which limits the accuracy when modelling the aft of a ship. For this reason, RANS is preferred over BEM. LES is a method which resolves the Navies-Stokes equations for the large eddies in the turbulent flow directly, thus providing more accurate results than the RANS method. For this reason, LES is sometimes used when modelling the flow around a ship model. This increase in accuracy also comes with an increase in computational cost, which is the reason why it is rarely used as part of an optimisation strategy. To reduce the computational costs the DES method was developed which makes use of a RANS method

with a turbulence model close to the surface of the model where resolving LES would be prohibitive and only resolves LES in the core turbulent region, where large turbulence scales play a dominant role [11]. Although this method does limit the computational costs these costs are still too excessive to be used in this project, thus the RANS method is preferred.

3.1.2. Propeller hull modelling

Extensive research has also been done into propeller-hull interactions without the goal of using an optimisation algorithm. For example [22] does research into gaining more insight into the different types of propeller losses for a propeller operating behind a Ship. While [25] and [30] examine different methods of modelling a propeller. [2] examines different types of propellers to gain insight into the effect different propeller designs can have on the propeller-hull interaction. The experience of this research can be used to help set up the simulation which will be used for the optimisation and help with modelling the propeller. The information provided by these papers can also help in analysing the resulting data from this project. To simulate the effects of the propeller the three methods which are used the most are the Actuator Disk representation in a RANS model, the BEM method or a full model of the rotating propeller in a RANS method. The RANS method is the same as described in the previous section which is also further explained in the section about CFD. The disadvantage of this method is that the propeller geometry is complex and the flow around a propeller is highly turbulent even with the risk of cavitation which requires unsteady simulations. To be able to properly compute this using the RANS method will require substantial computing power for each iteration. To combine the mesh around the hull and the mesh around a rotating propeller an overset grid method or a sliding interface technique needs to be implemented as shown in [23]. These techniques increase the computational load even further. Another method is BEM, BEM makes use of potential flow theory and is thus less computationally intensive than the RANS method. The coupling between the RANS model around the hull and the BEM model is explained in [17]. Both models are determined separately with the output of one model being the input of the other model, this process continues until the force imbalance between the thrust and the ship resistance is negligible. The last mentioned method is the Actuator Disk method, here the propeller is modelled using an actuator disk as described in [6]. The advantage of this method is that the actuator disk makes use of open water curves and thus requires very little computational capacity, while still capturing the global characteristics of the flow. The Actuator Disk method will be discussed in more detail in paragraph 4.1. Because of this the Actuator Disk method will be the preferred method to use in this research.

3.1.3. Optimisation

When performing a hull form optimisation the optimisation algorithm can either be directly coupled to the CFD code as done in [28] or can be linked using a surrogate model as done in [18]. With a directly coupled algorithm, the optimisation algorithm directly prescribes what parameter value will be used for the analysis. These optimisers are generally divided into global and local optimisers. Local optimisers are only capable of finding local maxima and minima around the initial design. For this reason, generally global optimisers are preferred, although they are generally more computationally intensive. One common algorithm used on the global scope is the Particle Swarm Optimisation (PSO) method [33]. This model makes use of continuous optimisation, continuously creating new variations based on information gained by previous variations till the design criteria are reached. This algorithm is categorised as a genetic algorithm, which makes use of neural networks to imitate evolution. The disadvantage of most evolutionary models is an increase in computational load.
Surrogate models as described in [18] create a response surface by analysing several predetermined variations on the model. The variations are usually determined with a sampling method of which Latin Hypercube Sampling is one of the more common methods. These sampling methods can be supplemented using data points that the designers of the experiment deem required to be part of the response surface. Afterwards, this response surface is used to create the surrogate model. For a single objective optimisation problem, the single fidelity Kriging method is most widely used to analyse this response surface [32]. If the results do not have the required accuracy and/or resolution additional variations around the optimum design can be added to improve the accuracy of the response surface.
Another optimisation strategy which is explored in [19] is the use of a multi-fidelity approach. The theory supporting this approach is that although a lower fidelity CFD method is not capable of predicting the design goal with the required accuracy, the method can be capable of predicting the relation between

the variations. The high-fidelity CFD method can next be used to add the required accuracy to the response surface around the optimum. This method might be preferable because a lower fidelity method costs significantly less computational time, thus saving computational time for the overall optimisation process. Making appropriate use of multi-fidelity optimisation methods however, requires extensive knowledge and effort to set up and thus falls outside the scope of this research.
To perform and manage the optimisation process the program HEEDS by Siemens will be used. HEEDS is a design space exploration and optimisation software which can interface with Rhinoceros, Grasshopper and STAR-CCM+. This program is chosen, because of its capability of interfacing with all the required software and previous positive experiences within the organisation. HEEDS can make use of the optimisation algorithm SHERPA, which makes use of multiple optimisation methods simultaneously and determines the participation of each method based on the effectiveness in the current optimisation problem [3]. The advantages of this algorithm are the increased efficiency compared to other optimisation algorithms and the ease of use when working with this algorithm.
An issue with the SHERPA algorithm is that it is not possible to gain insight into which sub-algorithm it uses at any given time. This does not allow for gaining insight into how the algorithm itself works which makes this algorithm not suitable as the base of this study. Because of this two studies will be run, one study with the SHERPA algorithm and one study with the NSGA-III algorithm [4] and the results will be compared. The NSGA-III algorithm is a multi-objective algorithm which performs a non-dominated sort on the combined population to determine the values for the next population. A more detailed explanation of how the NSGA-III algorithm works can be found in paragraph 4.3. This algorithm was chosen because it has provided good results in similar studies in the past even for single objective optimisation methods [24]. Another advantage of this algorithm is the fact that the algorithm itself provides an even distribution across the objective space without the need for specific inputs such as determining a mutation rate, which is necessary in a lot of genetic algorithms. This allows it to be used in a broad number of optimisation studies with minimal adjustments required. The two inputs which are required to be set are the population size and the number of generations. According to [24] the minimum population size to see any improvement using the algorithm is 4 since this is the minimum amount of design necessary to create a new population. However the HEEDS manual [12] recommends a minimum population size of 8 to be able to use the NSGA-III algorithm effectively. For this reason, the population size will be chosen as 8. The number of generations will be determined by an estimate of the amount of computational time which will be invested in the current study.

4

Theoretical background

In this chapter the background of the techniques used in this study will be discussed

4.1. Actuator Disk Model

As mentioned previously the propeller effects will be modelled using the Actuator Disk model. This paragraph will discuss how a propeller will be incorporated into a CFD analysis using the Actuator Disk model.

4.1.1. Flow effects

The Actuator Disk model can approximate the impact of the propeller on the axial and tangential flow acceleration. The proposed method is discussed in both [6] and [15]. With this method, the propeller is modelled as a thin infinite-bladed propeller which is represented in the grid as a disk with the diameter of the propeller. The thrust and torque produced by the propeller are introduced to the flow through pressure and velocity boundary conditions applied at the disk. These boundary conditions employ a uniform volume force distribution over the virtual. This distribution is called the Goldstein optimum which for the pressure jump can be described by the following equations:

$$\Delta p = A_x r^* \sqrt{1 - r^*} \tag{4.1}$$

Where A_x is defined as:

$$A_x = \frac{105}{8\pi} \frac{T(J)}{(R_P - R_H)(3R_H + 4R_P)} \tag{4.2}$$

Where $T(J)$ is the propeller thrust which is a function of the advance ratio J, which is defined as:

$$J = \frac{V_A}{n_p D} \tag{4.3}$$

with V_A being the advance velocity, which is the velocity of the fluid at the front of the propeller plane, n_p being the propeller rotation rate and D being the propeller diameter. $T(J)$ is determined using the open water curves of the Wageningen Ka series, R_P is the propeller radius, R_H is the hub radius and r^* is the normalised disc radius which is defined as:

$$r^* = \frac{r' - r_h'}{1 - r_h'} \tag{4.4}$$

Where $r' = r/R_P$ and $r_h' = R_H/R_P$. The tangential velocity jump boundary condition is determined using the following equation:

$$\Delta U_\theta = A_\theta \frac{r^* \sqrt{1 - r^*}}{r^*(1 - r^*) + r_h'} \tag{4.5}$$

Where A_θ is defined as:

$$A_\theta = \frac{105}{8\pi\rho}\frac{Q(J)}{U_X(R_P - R_H)(3R_H + 4R_P)} \tag{4.6}$$

Where U_x is the axial component of the velocity and $Q(J)$ is propeller torque as a function of J which is also determined using the open water curves.

4.1.2. Self propulsion computation

To determine the propeller rotation speed a self-propulsion computation will be performed as described in [14]. The goal of this computation is to find the point at which the ship resistance and the propeller thrust are in equilibrium. Two methods are proposed to achieve this. The first is to use a controller to change the propeller rotational speed. The second method is to compute the imbalance between the thrust coefficient K_T of the propeller and the required thrust coefficient K_T' determined by the total resistance of the model.
A typical proportional-integral controller which is used to achieve this goal is implemented as:

$$n_P = Pe + I\int_0^t edt \tag{4.7}$$

Where n_P is the propeller rotation rate e is the error and P and I are the proportional and integral constants. The error can be defined as:

$$e = R - T(J) \tag{4.8}$$

P and I require some computations to determine and R is the current total ship resistance. If these constants are not properly chosen overshoots and/or slow convergence may be the result. These constants can be chosen after simulations of the dynamic system behaviour using a simple model with an approximate propeller thrust curve and ship resistance and mass properties, with the propeller rotational speed controlled by the controller.
The second method numerically solves the following equation:

$$f(J) = K_T - K_T' \tag{4.9}$$

With K_T being determined by the open water curve of the propeller and K_T' is evaluated as:

$$K_T' = \frac{J^2 * R_{total}}{\rho_{InflowPlane} * V_{InflowPlane}^2 * D_P^2} \tag{4.10}$$

With $\rho_{InflowPlane}$ and $V_{InflowPlane}$ being the density and velocity around the inflow plane of the actuator disk and D_P being the diameter of this propeller. Once J has been determined using this method the Thrust and Torque provided by this actuator disk are determined using the following equations:

$$T = \frac{K_T * \rho * V_{InflowPlane}^2 * D_P^2}{J^2} \tag{4.11}$$

$$Q = \frac{K_Q * \rho * V_{InflowPlane}^2 * D_P^3}{J^2} \tag{4.12}$$

4.1.3. Determining propeller power

With the previously mentioned self-propulsion test, all the variables needed to compute the propeller power can be determined. As stated in [31] propeller power is calculated using the following equation:

$$P_P = 2\pi M_P n_P \tag{4.13}$$

Where n_P is the propeller rotation speed in rotations per second and $M_P = Q * \eta_r$, with Q being the propeller torque and η_r is the relative rotative efficiency, which can be assumed to be 1 for vessels propelled by twin propulsor pods. Q is also determined as a function of J using the open water curves of the Wageningen Ka series. Propeller power is related to two variables which are important in describing

propeller hull interaction the thrust coefficient t which describes the effect the propeller has on the ship resistance and is determined as follows:

$$t = \frac{T - R}{T} \tag{4.14}$$

With R in this case being the towing resistance of the ship. This relation is incorporated in the self-propulsion computation. The other variable is the wake fraction w which is determined as follows:

$$w = \frac{V_S - V_A}{V_S} \tag{4.15}$$

With v_S being the ship speed. This relation is part of the propeller power via the dependence between J and v_A, J being required to determine both T and Q

4.2. CFD

The CFD calculations will be done using the program STAR-CCM+, in this section, the physical principles behind these calculations will be discussed. Estimating and minimising the error and verifying and validating the calculations will also discussed here. Most of the information in this section is derived from [11] [14] and [5]

4.2.1. Governing equations

In this section, the governing equations determining the fluid dynamics will be discussed. These equations are based on the following conservation laws of physics:

- Conservation of mass: The mass inside a fluid is conserved.
- Newton's second law: The rate of change of momentum equals the sum of the forces on a fluid particle.
- The first law of thermodynamics: The rate of change of energy is equal to the sum of the rate of heat addition and to the rate of work done on a particle.

For hydrodynamics applications, it is assumed that the flow is incompressible with a Newtonian fluid and constant laminar viscosity throughout the flow. Because of the lack of change in density, there is no linkage between the conservation of energy and the conservation of mass and the momentum equations. Because of this the energy equations only need to be discussed when the analysed problem contains heat transfer. Since this is not the case for this research, only the mass conservation and momentum equations will be discussed.
Combined with the assumption of incompressible flow the continuity equation which describes the conservation of mass can be written as:

$$\nabla * U = \frac{\partial u}{\partial x} + \frac{\partial v}{\partial y} + \frac{\partial w}{\partial z} = 0 \tag{4.16}$$

Newtons second law for a Newtonian fluid can be described using the following momentum equations

$$\begin{aligned}
\frac{\partial(\rho u)}{\partial t} + \nabla(\rho u U) &= -\frac{\partial p}{\partial x} + \mu\nabla^2 u + \rho * f_x \\
\frac{\partial(\rho v)}{\partial t} + \nabla(\rho v U) &= -\frac{\partial p}{\partial y} + \mu\nabla^2 v + \rho * f_y \\
\frac{\partial(\rho w)}{\partial t} + \nabla(\rho w U) &= -\frac{\partial p}{\partial z} + \mu\nabla^2 w + \rho * f_z
\end{aligned} \tag{4.17}$$

These equations combined describe the fluid motion and can be used to predict the pressure and velocity of the fluid. The momentum equations can be separated into four distinct parts.

$$Timederivative + Convectiveterms = Diffusionterm + Forceterms$$

Where the convective terms describe the motions of the particles and the diffusion terms describe the internal forces and pressures. The force term describes external forces acting on the particle. These equations are also known as the Navier-Stokes equations and are the basis for most CFD methods.

4.2.2. Turbulence modelling

Turbulence is a natural state of fluid motion with coherent vortical motions called eddies. This is caused by interactions between inertia and viscous terms in the previously mentioned momentum equations. These equations technically apply to all scales of flow and thus are technically capable of describing all the complex interactions which create and describe turbulence. However, because of the complexity of the interactions it is in most cases not feasible to solve these equations for these cases analytically. A method to handle this issue is the use of the RANS method, this method makes use of time averaging to divide the flow velocity and pressure components between a mean and a fluctuating component as shown in the following equation:

$$\begin{aligned} U &= U(x,y,z) + U'(x,y,z) \\ P &= P(x,y,z) + P'(x,y,z) \end{aligned} \tag{4.18}$$

Where: $U(x,y,z)$ is the mean velocity and $U'(x,y,z)$ is the unsteady disturbance quantities in the flow such that $\overline{U'} = 0$. In a similar way $P(x,y,z)$ is the mean velocity and $P'(x,y,z)$ is the unsteady disturbance quantities in the flow such that $\overline{P'} = 0$. When inserting these in the Navier-Stokes equations, the so-called Reynolds stresses are formed with the form: $\tau'_{ij} = -\rho\overline{u'_i u'_j}$. Where i and j can be any of the three cardinal directions. These are extra stresses which arise because of the turbulent nature of the flow. To close the system of equations these Reynolds stresses need to be modelled. A way to model these stresses is by using the concept of turbulent viscosity, where the effects of the Reynolds stresses are modelled as a turbulent viscosity (μ_t). This viscosity is considered proportional to the turbulent velocity scale and the turbulent length scale. There are several approaches to determine a value for the length scale and the kinetic energy:

- Algebraic (0-equation) models: Uses an algebraic expression to determine the turbulent viscosity by relating the velocity and length scale to local flow conditions.
- 1-equation models: These models identify the velocity length scale with the turbulent kinetic energy (κ), creating one equation. The length scale is then related to the local flow properties.
- 2-equation models: these models use two separate transport equations to determine the velocity scale and the length scale. There are two popular versions of these models:
  - $\kappa - \epsilon$ model: here the viscosity is identified using κ and the turbulence dissipation rate (ϵ). This model is however generally limited to flows with high Reynolds numbers and a homogeneous turbulence structure, where the production and dissipation of turbulence are in balance. This model has undefined terms at the wall and thus needs to make use of wall functions, because of this it can perform worse close to the wall.
  - $\kappa - \omega$ model: here the viscosity is identified using κ and the specific turbulence dissipation rate (ω). This model can be integrated up to the wall without using wall functions however, this model is very sensitive to the free stream value of ω. Because of this spurious results can be obtained in both the boundary layer flows and free shear flows.

Because of the limitations of both 2-equations models the Shear Stress Transport (SST) model is created. This model uses a blending function to transition from a standard $\kappa - \omega$ model near the wall to a high Reynolds version of the $\kappa - \epsilon$ model in the outer portion of the boundary layer. This allows for accurate turbulence modelling up to the wall while also providing stable results in the rest of the computational domain.

4.2.3. Meshing

To perform a CFD analysis a three-dimensional grid needs to be created, there are two main types of grids, structured and unstructured grids. It is also possible to combine both grid types to create a hybrid grid. A structured grid can be created from different shapes of cells or one type of cell which consists of a fixed distribution of grid points in the three principal coordinate directions. A structured grid can also be locally refined. Because of the lack of flexibility generally a fixed grid needs more cells than an unstructured grid. An unstructured grid is generally created using one type of cell which can freely disform to be able to quickly generate a usable grid. The meshing time for an unstructured grid is reduced compared to a structured grid.
The quality of the mesh is dependent on the following factors:

- Size of the cell: the discretisation error reduces with a reduction in cell size. A trade-of needs to be made between computational time and the size of this error
- Smoothness: When there is a difference in cell size the change should be smooth
- Skewness: This needs to be limited since highly skewed cells will have trouble with the diffusion of physical quantities between cells
- Aspect ratio: The closer to one the better the results of the mesh

To find the quantities of these values which allow an accurate enough analysis a grid refinement study can be performed. The process for this will be explained in the next paragraph.

4.2.4. Grid refinement study

A part of the discretisation error is affected by the size of the grid used, where larger grid elements correlate with an increase in the error size. Grids with smaller elements require more computational power and time to perform an evaluation however. To find the right balance between these two factors a grid refinement study will be performed. Usually with grid refinement studies it is assumed that the discretisation error can be represented by a single-term power series expansion [7] [10] [8] [14] [21].

$$\phi_i = \phi_0 + \alpha h_i^p or \phi_i = \phi_0 + \alpha h_1^p \left(\frac{h_i}{h_1}\right)^p \tag{4.19}$$

Where ϕ_i is the value of the quantity of interest from grid number i, ϕ_0 is the estimated exact solution for the quantity of interest, α is a constant and p is the observed grid convergence. Two methods will be used to perform the grid refinement study. primarily the newest method implemented in the Numerical Uncertainty Analysis tool of MARIN will be used [29]. However, a simpler Richardson extrapolation will also be performed as a check.

The Richardson extrapolation method makes use of three different grid sizes which are refined by a constant grid refinement factor. For three-dimensional grids in CFD research a grid refinement factor of $\sqrt{2}$ is common practice. With this method, p is predicted using the following equation:

$$p = \frac{ln\left(\frac{\phi_3 - \phi_2}{\phi_2 - \phi_1}\right)}{ln(r)} \tag{4.20}$$

With ϕ_3,ϕ_2 and ϕ_1 being the coarse, medium and fine mesh respectively and r is the grid refinement factor. With an estimation for p, the exact solution will be estimated as follows:

$$\phi_0 = \phi_1 + \frac{\phi_1 - \phi_2}{r^p - 1} \tag{4.21}$$

Because this method only makes use of three different grid sizes it is less accurate than other methods. The method used in the Analysis tool makes use of multiple steps [9]. The first step is to use the least squared method to solve equation 4.19. Which can be performed by minimising the following function:

$$S(\phi_0, \alpha, p) = \sum_{i=1}^{n_g} w_i(\phi_i - (\phi_0 + \alpha r_i^p))^2 \tag{4.22}$$

With w_i being a weight which is added to have the finer more accurate meshes have more effect on the results than the coarser meshes. The method makes use of four different weight distributions:

- Constant weights:

$$w_i = \frac{1}{n_g} \tag{4.23}$$

  with n_g being the number of reviewed grids

- weights dependant on $\frac{1}{r_i}$:

$$w_i = \frac{\frac{1}{r_i}}{\sum_{w_i=1}^{n_g} \frac{1}{r_{iw}}} \tag{4.24}$$

with r_i being the grind refinement factor $r_i = \frac{h_i}{h}$

- Huber weights:

$$W_i = \begin{cases} 1 & \Leftarrow |e_i| \leq k \\ \frac{k}{|e_i|} & \Leftarrow |e_i| > k \end{cases} \tag{4.25}$$

- Tukey (Bisquare) weights:

$$W_i = \begin{cases} \left[1 - \left(\frac{|e_i|}{k}\right)^2\right] & \Leftarrow |e_i| \leq k \\ 0 & \Leftarrow |e_i| > k \end{cases} \tag{4.26}$$

In equation 4.25 and equation 4.26 $|e_i|$ is the absolute difference between the data value and the fitted line and k is a factor from the median of the $|e_i|$ distribution M_e:

$$k = \begin{cases} 1.994 M_e & \Leftarrow Huber \\ 6.946 M_e & \Leftarrow Bisquare \end{cases} \tag{4.27}$$

The values of W_i are normalized using the following equation:

$$w_i = \frac{W_i}{\sum_{iw=1}^{n_g} W_{iw}} \tag{4.28}$$

The weights defined by the Bisquare method can be equal to zero, to prevent this an extra criterion is added: the weight applied to the finest grid must be larger than or equal to 0.1 which can be written as $w_1 \geq 0.1$ If one or more of these equations satisfy the following condition: $0.5 \leq p \leq 2$ then the results of this equation will be used. If more weight distributions satisfy the condition the one with the smallest standard deviation will be used which is given by:

$$\sigma_{udisc} = \sqrt{\frac{n_g XS}{n_g - 5}} \tag{4.29}$$

If none of the weight distributions satisfy the conditions the alternative power series expansions will be performed. Which are expanded upon in [9].

4.2.5. Time step computation

To determine the correct value for the timestep the ITTC has written down several guidelines. There are different guidelines for explicit and implicit solvers, for explicit solvers it is recommended that a fluid particle is not able to travel the distance of more than one cell in a single timestep. While the timestep for an implicit solver can be greater. The maximum allowable timestep can be described using Courant-Friedrichs-Lewy (CFL) number, also known as the Courant number:

$$\frac{|\overline{u}|\Delta t}{\Delta x} < C_{max} \tag{4.30}$$

Where $|\overline{u}|$ is the local velocity, in resistance simulation this value is usually taken as the ship velocity. Δt is the timestep and Δx is the linear cell size in the flow direction. C_{max} is the maximum allowed Courant number, for explicit solvers this number is one, while this number can be larger for implicit solvers. The two relevant rules of thumb for implicit solvers for this project are:

- For complex unsteady phenomena, use at least twenty time steps per period for the highest frequency to be resolved.
- Δt must be smaller than 0.01 L/U if one or two equation turbulence models are used [14]. With L being a length scale, generally the ship length and U being a velocity scale, generally the ship speed.

4.2.6. Boundary conditions

There are two main types of boundary conditions which can also be combined to provide multiple different boundary conditions. There are Dirichlet boundary conditions which specify the distribution of a physical quantity over the boundary at a given time step and Neumann conditions, which define the distribution of the first derivative of a physical quantity. In the proposed project there are several areas which need boundary conditions:

- Inflow: both the model of the full ship and the model of the aft of the ship require Dirichlet boundary conditions at the inflow which impose a certain velocity and pressure over the boundary.
- Outflow: for the outflow typically a Neumann condition which imposes a gradient of zero is implemented.
- Symmetry plane: for the longitudinal symmetry plane a symmetry boundary condition will be implemented, which states that the normal velocity and the normal gradients of all variables are zero at the plane. This boundary condition is thus a combination of both types.
- Other boundaries of the computational domain: for the other boundaries of the computational domain usually a symmetry condition is imposed as well, however an imposed velocity could also be implemented.
- Hull: The hull will be modelled as a wall, usually a non-slip boundary condition is employed at the wall which imposes the wall velocity for the tangential fluid velocity, which is zero in this project.

4.2.7. Errors and uncertainties

The RANS model is an approximation concerning the fluid flow in reality, because of this several uncertainties and errors are inevitable. An error can be described as a recognisable deficiency which is not caused by a lack of knowledge, while an uncertainty is caused by a lack of knowledge. A numerical method is classified as stable when the error that appears in the solution is not amplified, while in an unstable method, an error will cause a disturbance which will either grow indefinitely or create large oscillations in the results. The following possible types of errors may occur:

- Discretization or numerical errors: Because of the discretization process all solutions will be an approximation. These errors are the difference between the exact solution to the equations and the numerical solution derived from the grid. A couple of things can be noted to be a cause of these errors: truncation errors are caused by approximation; the smaller the grid size the smaller this error will be, theoretically this error should become zero when the grid size becomes zero; the use of higher order schemes can rapidly decrease this error
- Round-off errors: Because computers can not store a number with infinite decimals, rounding of numbers is forced. Generally, these errors are not of great significance
- Iterative or convergence errors: Is the error caused by the lack of convergence when the program has reached a previously set limit with regards to convergence. This limit is usually determined using residuals which indicate how far the solution is to perfect conservation of mass and momentum. The ITTC guidelines recommend the following criteria ”*the drop of scaled residuals by at least three orders of magnitude off their initial values*”. However, depending on the type of analysis different convergence criteria can be chosen.
- Model error and uncertainties: The errors are caused by the fact that instead of the exact governing equation a physical model is used. This model might not be a good representation of reality. For RANS simulations with turbulence, the turbulence model is a common cause of errors.
- User and code error: These are errors created by the user, either due to lack of experience or due to human error. The software itself also causes errors, these can be in the shape of bugs. The chance of software errors is increased if the software is used for use cases for which it is not verified.

These errors and uncertainties can be estimated using the guidelines provided by the ITTC [14].

4.3. NSGA-III algorithm

The NSGA-III algorithm is an adjusted version of the NSGA-II algorithm to make the algorithm suitable as a many-objective optimisation algorithm [4]. The NSGA-II algorithm works according to the following principle. When considering the t-th generation, the parent generation is P_t which has a size of N and the offspring population from P_t is Q_t which also has a size of N. N being the population size. The algorithm first chooses the best N members of the combined parent and offspring population called R_t allowing the algorithm to preserve elite members of the parent population. The best N members are chosen by sorting R_t along different non-domination levels called F1, F2 and so on. Then each non-domination level is selected one at a time to construct a new population S_t starting from F1 and stopping when S_t is larger or equal then N in size. All the solutions from the other levels will be discarded. In most situations the last level is only partially accepted, in that case only the solutions that will maximise the diversity of this last front are chosen. The way this is achieved is different for the NSGA-III algorithm. The NSGA-III algorithm uses a predefined set of reference points to ensure diversity. The algorithm first constructs the ideal point $\tilde{z}$ by identifying the minimum value of each objective. Next, the algorithm constructs a hyperplane from the most extreme values of each objective. An example for a three-objective problem can be seen in figure 4.2. The reference points are either constructed or projected on

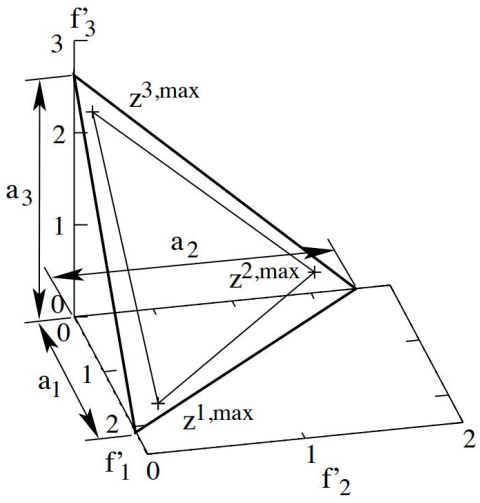

Figure 4.1: Example of hyperplane constructed by NSGA-III algorithm [4]

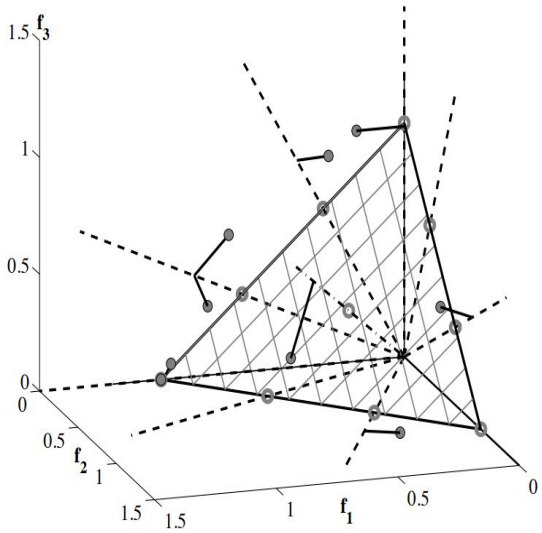

Figure 4.2: Example of reference lines constructed by NSGA-III algorithm [4]

this hyperplane. Next, each population member will be associated with a reference point. To determine this association a reference line is constructed between each reference point and the origin of the the hyperplane. Next, the perpendicular distance between each population member and the reference line is determined. The reference point for which this perpendicular distance is the smallest will be associated with this population member. Figure 4.2 demonstrates this process with the same three-objective problem. To choose which of the population members of the last level will be added to the new population a niching algorithm will be used. This algorithm selects the reference point with the least amount of chosen population members associated with it. When a member of the last population level is associated with this reference point this member will be added to the new population. When there are no population members associated with this reference point this point will be skipped and the next reference point with the least population members associated with it will be chosen. This process continues until the next population is of size N. Finally, a new offspring population is created from this new parent population and the process can start anew. A more detailed explanation can be found in [4].

II

Preparations

5

Construction of the parametric model

In this chapter, the parametric model created using Grasshopper and RhinoCeros will be explained. The parametric model generates a 3D model of the aft ship of the vessel which gets joined with the front part of a vessel which was designed in a previous design round by Vuyk Engineering. Next, this model is exported to a .igs file which can be used as an input for the CFD simulations. The model is based on four plates: The bottom plate, the side plate, the aft ascending plate and the transom. The following nine parameters are used to transform these flat plates into the aft of the vessel.

- Depth: Determines the depth of the vessel
- Aft Arc Angle (β): Determines the angle at which the arc of the bottom from the transom is created as illustrated in figure 5.1
- Transom Height (h): Determines the height of the centre of the transom as illustrated in figure 5.2
- Aft Ship Angle (α): Determines the angle between the centre of the transom and the keel as illustrated in figure 5.3
- Aft Ship Length: Determines the length of the aft part of the vessel
- Breadth: Determines the breadth of the vessel
- Transom Angle (t): Determines the angle at which the transom rises to the side of the vessel as illustrated in figure 5.2
- Bottom Radius (R): Determines the radius between the bottom and the rising aft of the vessel as illustrated in figure 5.4
- Bilge Radius (r): Determines the bilge radius as illustrated in 5.5

Of these parameters Aft Arc Angle, Aft ship angle, Transom Angle and Bottom Radius were determined to have the most significant effect on the hullshape and for this reason will be used as inputs for the optimisation algorithm. This determination was made based on previous studies and the experience of engineers at Vuyk Engineering.

5.1. RhinoCeros Checks

The running of a RhinoCeros analysis is a lot faster than running a STAR-CCM+ analysis, because of this as many checks as possible have been implemented in RhinoCeros to prevent STAR-CCM+ from running when a model is infeasible. This approach was taken on top of limiting the range for the input variables to make sure mostly feasible designs are analysed. This is necessary since it is infeasible to limit the range for the input variables in such a way that only feasible designs are analysed while also allowing the optimisation algorithm to analyse the full range of possible designs.

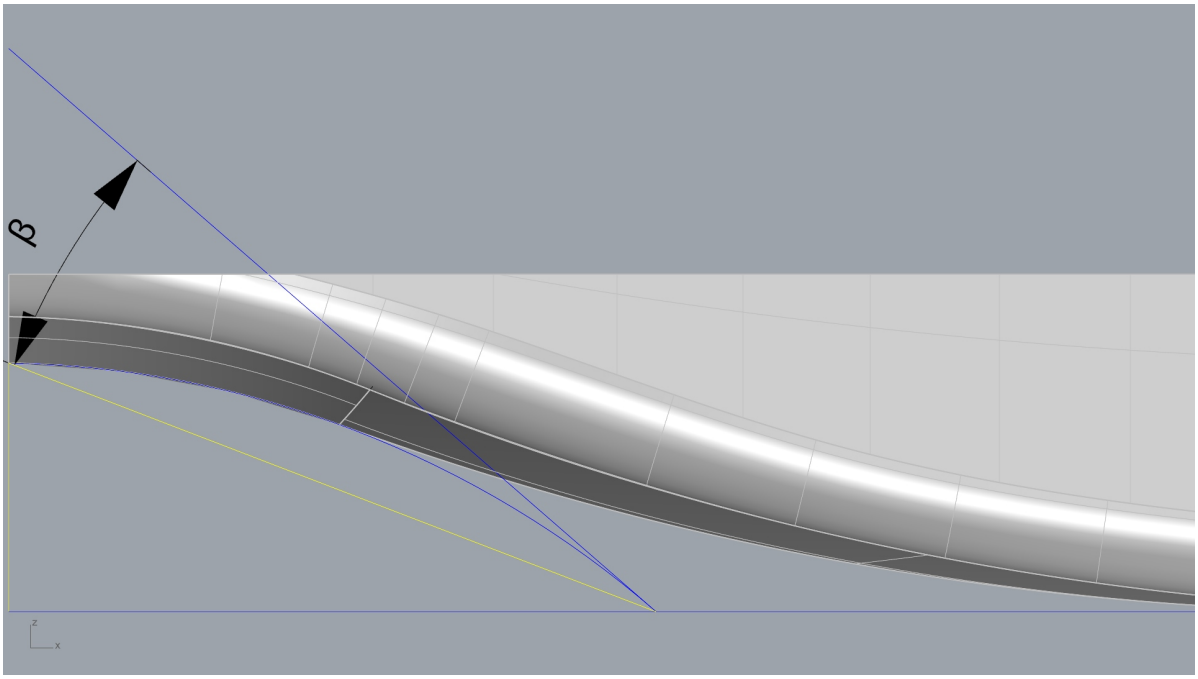

Figure 5.1: Illustration of how the Aft Arc Angle affects the parametric design

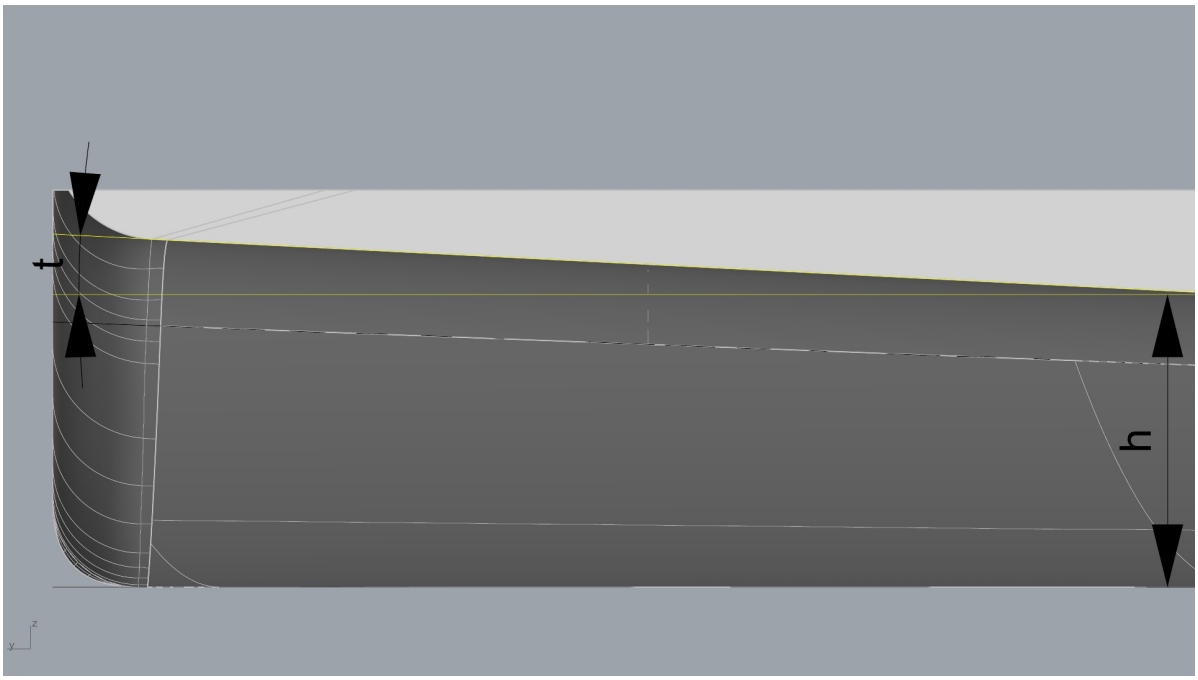

Figure 5.2: Illustration of how the Transom related variables affects the parametric design

- The first check is the propeller clearance check: Since the position of the propeller is fixed in STAR-CCM+ an element was implemented in RhinoCeros which checks if the proposed vessel shape has enough clearance around the propeller. The values for the propeller clearance recommended by Wärtsilä [1] were used.
- A check to count naked edges was implemented, this function checks if there are any naked edges in the design. This indicates if the model is fully closed since a fully closed model does not have any naked edges. When naked edges are detected HEEDS can prevent STAR-CCM from simulating a not fully closed model.

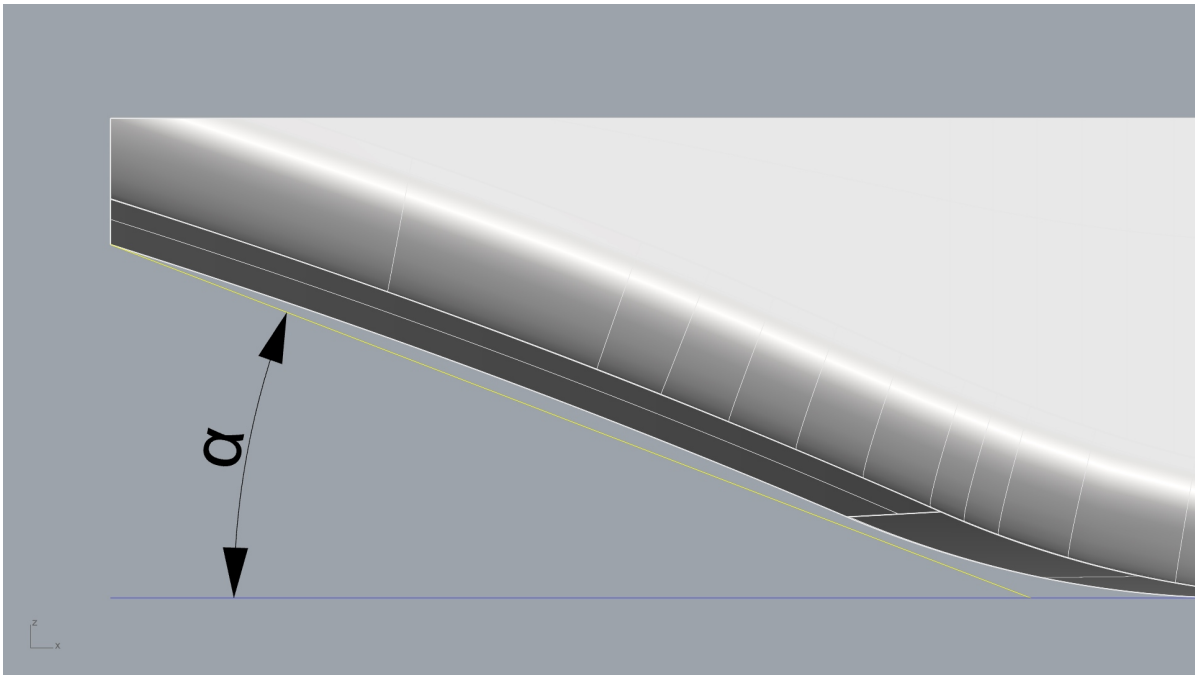

Figure 5.3: Illustration of how the Aft Ship Angle affects the parametric design

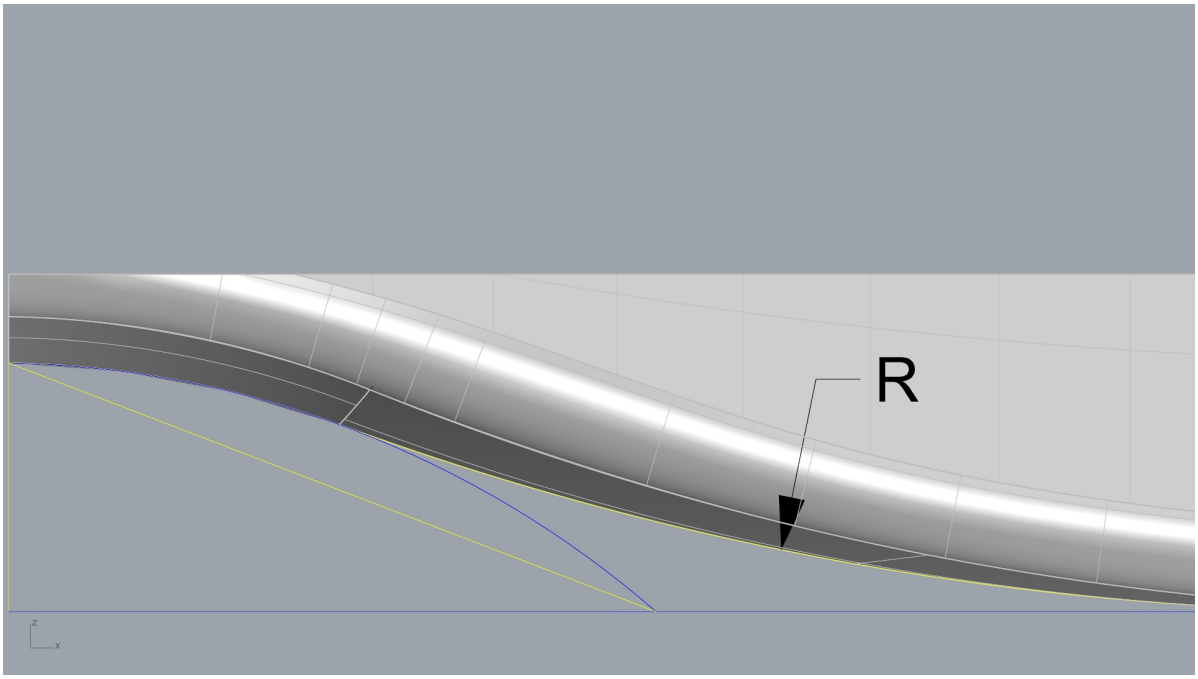

Figure 5.4: Illustration of how the Bottom Radius affects the parametric design

- A function was added which determines the volume of the model. This output serves two purposes. First, this allows HEEDS to not analyse vessels which have a significantly lower volume than the target volume since these vessels will not be able to perform the stated function of the vessel. The second purpose is to be used as an input for the correction function. The specific use of the volume correction function will be explained in chapter 9. This check was made redundant by the function which determines the required draft of the vessel which is described in paragraph 11.1.

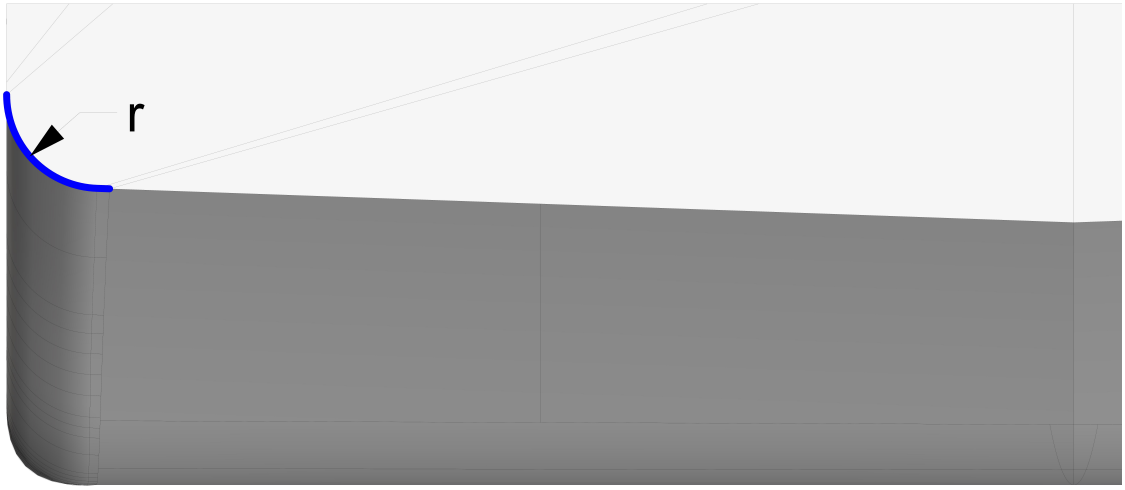

Figure 5.5: Illustration of how the Bilge Radius affects the parametric design

6

Approach CFD computations

In this chapter, the chosen approach to perform the CFD computations will be discussed. While the Design and the choice for the geometry are discussed in chapter 5, this chapter will elaborate on the other set-up choices made inside STAR-CCM+ to perform the CFD computations

6.1. Domain

The chosen domain, in CFD research, commonly referred to as the virtual towing tank makes use of the dimensions as prescribed by the ITTC [14]. Which are:

- Width extends $1.5 * L_{ship}$ besides the ship
- Length extends $1.5 * L_{ship}$ in front of the ship and $2.25 * L_{ship}$ behind the ship
- Depth extends $1.5 * L_{ship}$ below the ship

6.2. Mesh generation

The shape and size of the mesh are of great influence on the convergence and the solution of the CFD analysis. Because of this care needs to be given to how the volume mesh is generated. Because of their robustness, a structured volume mesh is used for this research. The rest of this paragraph will explain the steps and measurements taken for these CFD computations.
To start the surface is meshed using the surface remesher tool in STAR-CCM+. This tool re-triangulates the starting surface of the vessel and automatically repairs the surface if necessary. Next, the underwater section of the computational domain is meshed using a tetrahedral mesher. Which provides a mesh which is aligned with the free surface. This improves the performance of the mesh in a multiphase flow model. Next, a trimmed cell mesher is used to complete the meshing of the rest of the computational domain. This mesher cuts the previously generated mesh with the surface of the geometry instead of stretching or compressing cells to fit. The default growth rate for the cells has been set to slow, which helps mitigate wave reflections caused by an abrupt change in cell size.
To resolve the boundary layer, a prism layer mesher is used to resolve the flow near the hull with a non-slip boundary condition. This mesher creates an offset from the hull surface which is trimmed upon the volume mesh. Depending on which wall functions are used the choice for target y+ value can be made. These choices will be discussed in another section.

6.3. Physics models

For every CFD simulation, a choice needs to be made for which physics models are chosen to simulate. Most of the possibilities were discussed in chapter 3. This paragraph will give an overview of the physics models which were chosen for this simulation. A more detailed explanation of the chosen models can be found in the STAR-CCM+ user guide [26].

- RANS: As previously discussed, this simulation will make use of a Reynolds-Averaged Navier-Stokes model.

- Realizable K-ϵ Two-layer Turbulence model: although in the research it was found that the SST turbulence is the most robust turbulence model. The choice was made to make use of wall functions to save on computational time. Because of this and because the support system from Vuyk Engineering already has good experience with the K-ϵ model the choice for this model was made. Other turbulent flow models are described in paragraph 4.2.2. However, to regain some of the robustness the Two-layer turbulence model was chosen which divides the model into a layer near the wall and a layer further away from the wall. Where in the layer near the wall the turbulent dissipation rate ϵ and turbulent viscosity μ_t are specified as a function of wall distance.
- Cell Quality Remediation: this model identifies poor quality cells based on multiple criteria such as the skewness angle and improves these properties. This model is especially helpful in an automated workflow since an engineer will not be able to investigate and improve the mesh before the CFD simulation.
- Gravity: a gravity model is used to account for the gravitational acceleration
- Implicit Unsteady: In the case of a segregated flow an implicit unsteady model must be applied to control the time step and the iteration update.
- Multiphase flow and interaction model: Because the choice to not model the free surface will need to be verified. To perform this verification a multiphase flow and interaction model is implemented. To model both the density and viscosity of the seawater and air.
- Segregated flow model: The segregated flow model solves the momentum and mass equation sequentially and solves the non-linear governing equations iteratively for each solution variable one after the other.
- Three-Dimensional model: Since this is a three-dimensional simulation a Three Dimensional model is chosen to be used
- Two-Layer all y+ wall treatment: The wall treatment is a set of assumptions which together form the wall functions. The all y+ wall treatment combines the classical wall functions for high y+ prism layers and the models which resolve up to the wall for low y+ prism layers. Making it a robust wall treatment which can be used for every kind of prism layer.
- Virtual Disk model: This model includes a Propeller in the simulation. The propeller is modelled as an Actuator disk. This model makes use of Goldstein's optimum to determine the thrust and torque distribution for the effects the propeller has on the volume. The theoretical background is explained in section 4.1.
- Volume of Fluid: The volume of fluid model models the interaction between the two fluids and thus models the behaviour of the free surface.
- VOF wave model: This model simulates gravity waves in a light fluid heavy fluid interface such as the seawater air interface in this simulation.

6.4. No Free surface set-up

A verified CFD method was already in use by Vuyk Engineering for simulating a towing test for a Full-scale vessel while simulating the free surface and air-seawater interaction. Because of this, this model was used as the base case to verify the choice to not model the free surface in the optimisation study. To keep the comparison as close as possible this method was also used to create the model which does not simulate the free surface. This was achieved by reducing the computational domain to only include the submerged part of the hull and virtual towing tank and changing the top boundary to a wall boundary with full slip conditions.

6.5. Stopping criteria

As stated previously this simulation will be used in an optimisation analysis. Because of this extra care is taken in selecting the stopping criteria for this simulation. The stopping criteria are several criteria

which together determine if a simulation has been completed and the results have converged to a reasonable level. To check for this convergence an Asymptotic Limit criterium is used which checks if maximum and minimum values of the resistance over several iterations remain between a specified range.
To prevent the server from continuing calculation which for some reason will not converge three other criteria are added:

- Maximum physical time criterion: this criterion checks if the simulation has passed the maximum physical time which has been simulated. This prevents a simulation from running long passed the expected time necessary for this simulation.
- Vmax monitor criterion: This criterion checks if the local velocities are above an expected value. This is an indicator that a simulation is diverging and thus will not converge to a reasonable solution

6.6. Input virtual disk

The input for the virtual disk has been directly or indirectly modified in a couple of ways.
First, the open water curve for the propeller has been selected. This open water curve has been selected using the optimisation tools from Vuyk Engineering and the open water curves from the Wageningen ka 4-70 propeller with the 19a ducted nozzle. This specific propeller was chosen because of the positive experience previous designers had with this type of propeller when working on similar vessels. The specific P/D which has been used for this study has been determined using the resistance estimation from a previous design phase, while the diameter is based on the propeller clearance needed for the reference design. This has resulted in a P/D of 1.35 and a diameter of 5.2m.
The mean total resistance is used as the input for the ship resistance to determine the required propeller thrust. During the first five time steps the total resistance is approximately a factor of 20 larger than the converged resistance. To prevent this peak in resistance from affecting the mean total resistance during the start of the simulation the first five time steps will be excluded from this parameter. This way the results for the required propeller power can converge faster and use less computational resources.
As mentioned in chapter 2 the resistance determined by the CFD simulation without a free surface will not determine the total resistance the propeller thrust will have to overcome. This is because the wave-making resistance and air resistance are excluded from this simulation. Because the required propeller thrust is determined using the total resistance the propeller experiences an estimation for the wave-making resistance and air resistance have been added to the equation which determines the required propeller thrust. The goal of adding this estimate is to make sure the propeller operates at a point which would be closer to the real operation point of the propeller. The air resistance has been estimated using a previous simulation made by Vuyk Engineering. The wave-making resistance will be estimated using the method proposed by Holtrop Mennen [13].

6.7. Simulation outputs

Because this simulation is made to work for an optimisation study certain outputs will be automatically generated to be able to review every design during the optimisation study.
The following plots are generated:

- A plot of the residuals plotted against the number of iterations
- A plot of the pressure and friction resistance
- A plot of the total resistance and the mean total resistance
- A plot of the propeller thrust and torque
- A plot of the J value and rpm of the virtual disk
- A plot of the local velocity around the rim of the virtual disk

These plots allow for the review of individual designs. Especially if an error occurs can these plots give insight into what might have caused this error. To also help with this an image is created of the three-dimensional view of the mesh around the aft of the vessel and an image of the local velocity over the virtual disk entry plane.

7

Time step and grid refinement

In this chapter, the methods which were described in chapter 3 will be used to determine the setting which will be used in the definitive simulation.

7.1. Time Step

Based on the the ITTC guidelines [14] and the experience of fellow engineers working for Vuyk Engineering the choice was made to not perform a time refinement study, but to define the timestep as:

$$\Delta t = 0.01 * \frac{L_{vessel}}{V_{vessel}} \tag{7.1}$$

Where L_{vessel} is the length of the vessel and V_{vessel} is the target velocity of the vessel. This definition for the timestep has in previous CFD simulations proven to limit the discritization error caused by the choice of timestep.

7.2. Grid Refinement

To gain insight into the discretization error caused by the grid size the choice was made to perform a grid refinement study. The Richardson extrapolation method was used initially to give an indication of which grid size could be used in further calculations. At a later time, the MARIN verification tool was used to perform a more in-depth grid refinement study. Both methods are described in chapter 3. A grid refinement factor of $\sqrt{2}$ was chosen and five grid sizes were evaluated. The results from the Richardson extrapolation can be found in 7.1 and the results from the MARIN verification tool can be found in 7.2. The data can be found in appendix A.

Based on this data the choice was made to continue with the finest grid which corresponds with a discretization error caused by the grid size of 3.6%. This grid size was chosen in part for the reason that the expected improvement in design by the optimization algorithm is limited. Because of this limiting the calculation error will increase the chance of a significantly improved design being found, by lowering the limit for this significant improvement. This does increase the computational time, however the total required computational time has been limited with other choices and improvements.

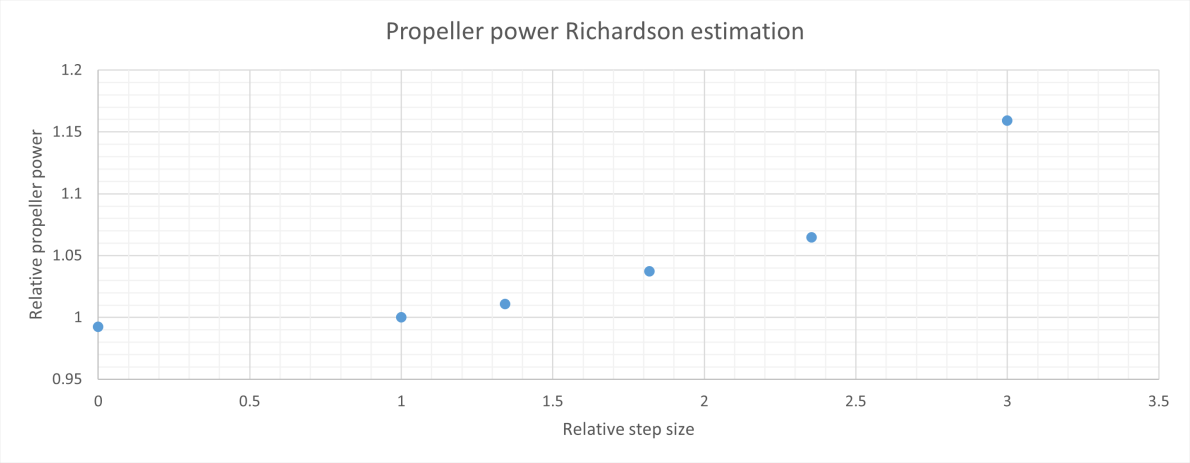

Figure 7.1: Results from the Richardson estimation

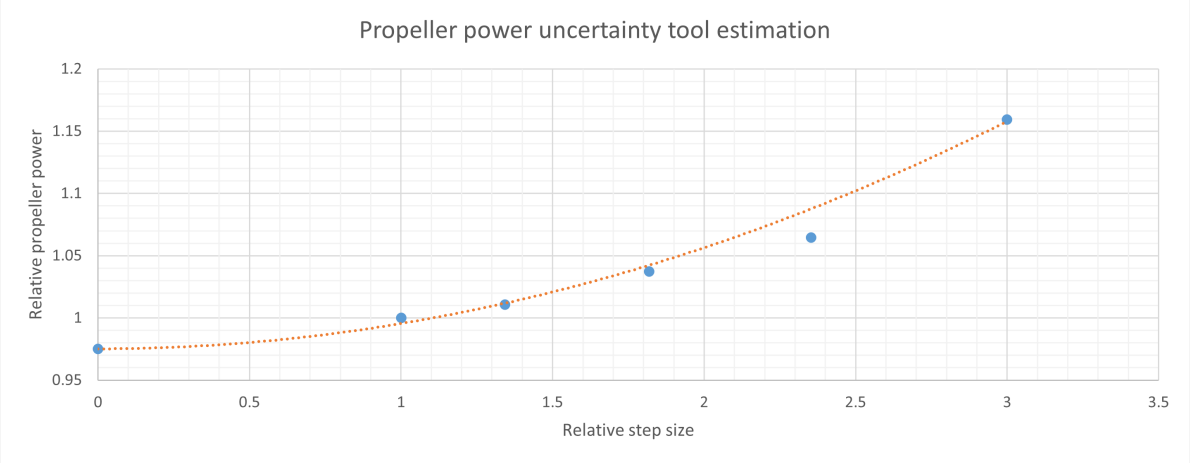

Figure 7.2: Results from uncertainty tool by MARIN

8

Partial ship analysis assumption

As stated in chapter 2 to save computational time the option to simulate only the aft half of the model has been explored. To properly verify this assumption first the effects of not including the free surface have been analysed and after having found this assumption acceptable the effects of only simulating the aft half of the model have been analysed

8.1. Effects of not including the free surface

Because the focus of this research is on the interaction between the hull and the propeller the difference in local velocity around the propeller has been analysed. To achieve this two additional analyses have been done, both without the propeller, one including the free surface, while the other one excludes the free surface. These analyses allow the comparison of the effect which the hull will have on the propeller in both situations while they exclude the effect the propeller itself will have on the local velocity. The results can be seen in figures 8.1a and 8.1b These graphs display the local velocity at the tip of the

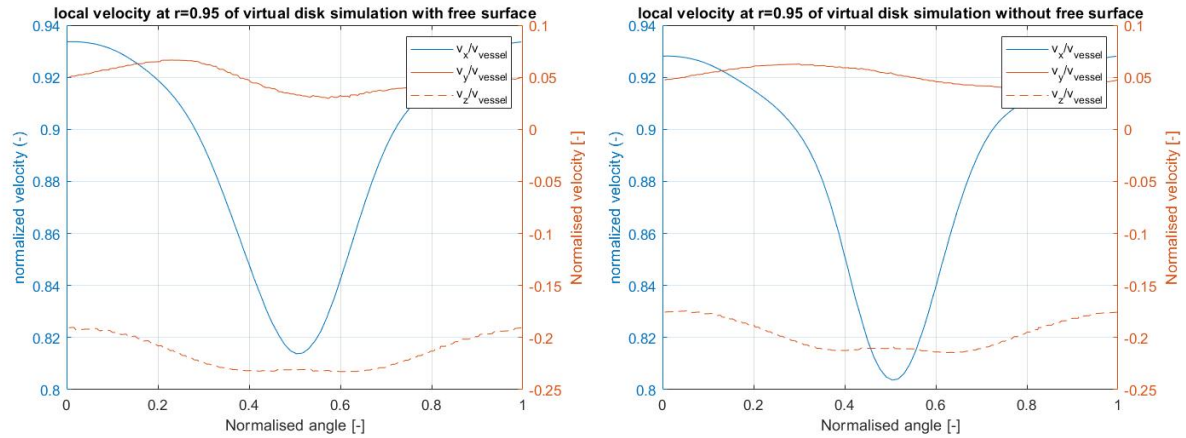

(a) Local velocity around propeller radius in simulation including the free surface

(b) Local velocity around propeller radius in simulation excluding the free surface

Figure 8.1: Comparison of the local velocity on the inflow of the virtual disk between a simulation including the free surface effects and a simulation excluding the free surface effects

propeller, which is the area of the propeller which is most affected by the inflow velocity. As can be seen, while both figures are not identical, they do match closely. This supports the hypothesis that not modelling the free surface will not have a significant effect on the inflow of the virtual disk. Not modelling the free surface does however influence the total resistance experienced by the vessel. This is because when excluding the free surface effects the wave-making resistance is also excluded. This difference in resistance influences the working point of the propeller. Because of this, an estimation of the wavemaking resistance has been made using the method of Holrtop and Mennem [13]. This

predicted wave-making resistance was however significantly larger than the difference in resistance between the two simulations. The most likely cause for this difference is the fact that the proposed vessel design is outside of the original scope of the vessels the Holtrop Mennen estimation has been based on. To correct for this difference in resistance estimations a correction factor c was determined using the following equation

$$c = \frac{R_{difference}}{R_{W,Holtrop-Mennen}} \tag{8.1}$$

where $R_{difference}$ is the resistance difference between the simulation with the free surface included and the simulation with the free surface excluded and $R_{W,Holtrop-Mennen}$ is the wave-making resistance predicted by the Holtrop-Mennen estimation. The correction factor which resulted from this equation was 0.194.

8.2. Partial CFD analysis

Having verified the assumption of excluding the free surface the choice to only simulate the aft half of the ship will be investigated. To achieve this an analysis of the full vessel was performed without incorporating the effects of the free surface. All the local velocities in the domain were recorded in a plane at half the ship length. These local velocities were then imported and used as the values for the velocity input in a new simulation in which the computational domain was limited to only the aft half of the vessel. The velocity input does not allow for an input of the locale pressures. This set-up however did not result in a successful analysis. The difference between the input velocity and the velocity in the other cell was too great for the solvers to be able to resolve, which caused a computational error. The exact cause for this error can be further investigated in another study.

Another method which was tried to perform the half analysis was to use the ship velocity as the input velocity for the half-ship plane. This method resulted in a pressure resistance which was significantly larger than in the full ship simulation. This is caused by a significant negative pressure coefficient along the surface of the hull as can be seen in figure 8.2 This pressure coefficient is significantly smaller than

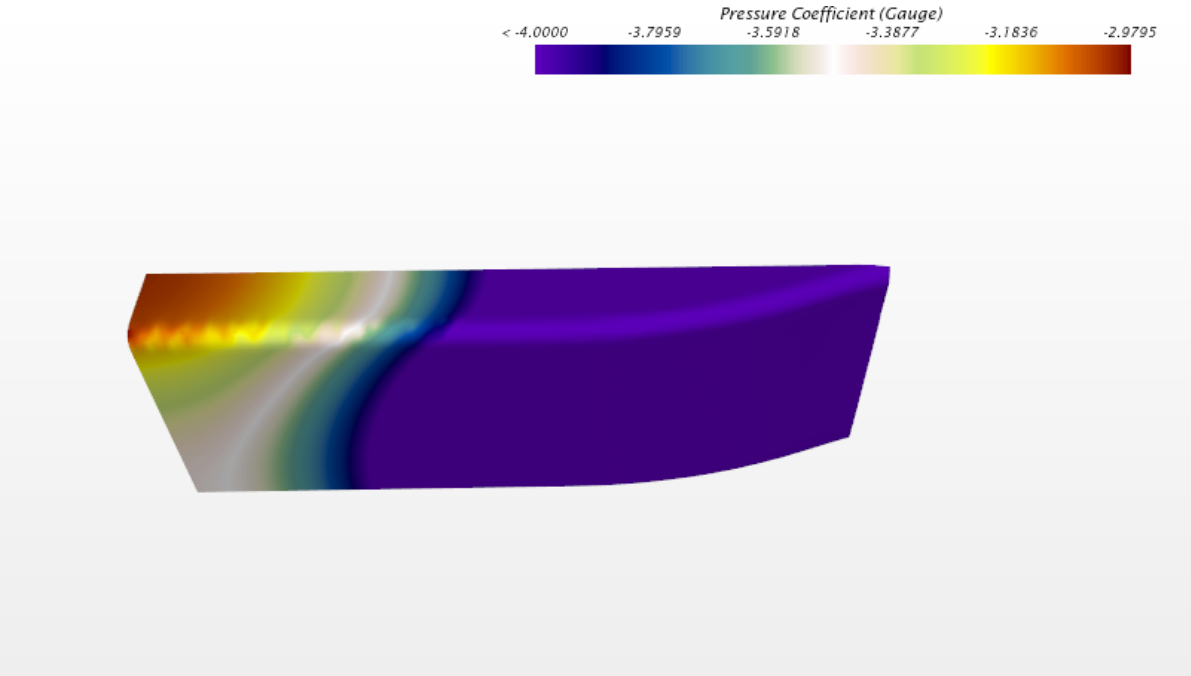

Figure 8.2: Pressure Coëfficient along the partial hull

the pressure coefficient along the hull in the full hull simulation which is shown in figure 8.3 The current hypothesis about the cause of this phenomenon is that the lack of unobstructed space for the flow to fully develop causes a drop in pressure along the hull. However further investigation will be necessary before drawing any definitive conclusion.

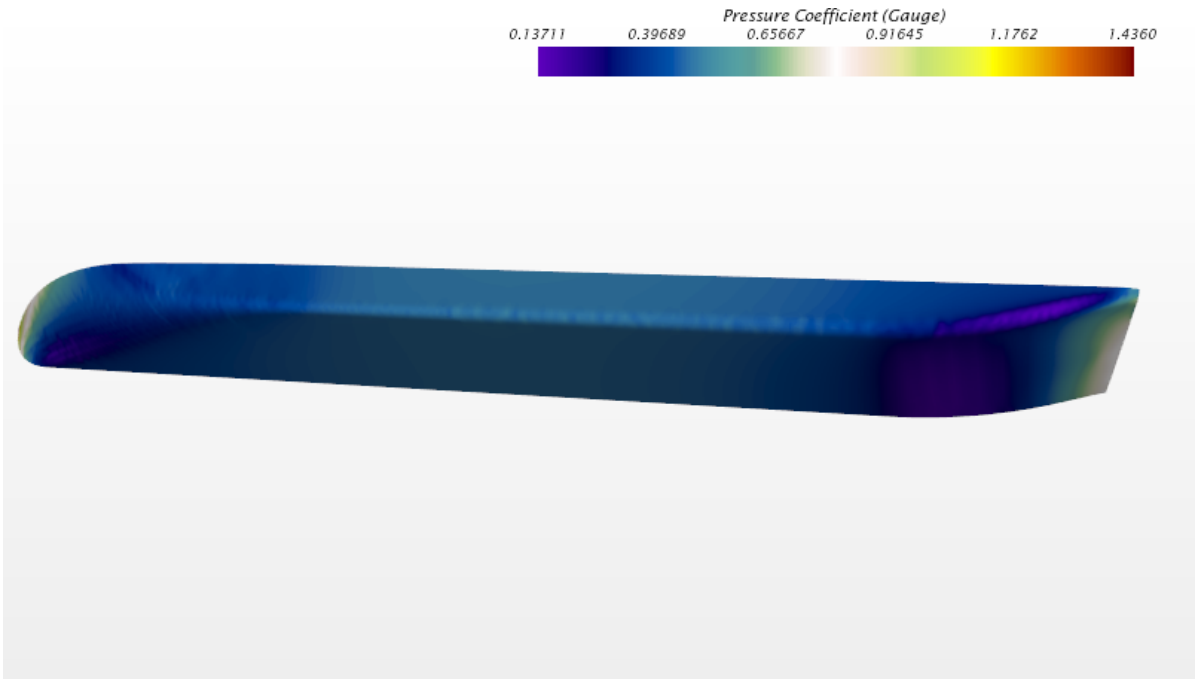

Figure 8.3: Pressure Coefficient along full hull

9

Settings for HEEDS

The parametric model and the CFD simulation are both controlled by the program HEEDS which manages the workflow which was described in chapter 2. The settings and outputs created by the individual parts of the workflow have been discussed in previous chapters. This chapter will explain the technical settings which have been used to make HEEDS work as a workflow manager and optimisation tool.

9.1. Checks and corrections

Several checks and corrections have been introduced to prevent the optimisation algorithm from trying to generate further designs based on an error design.

9.1.1. Volume check

As stated previously the wetted volume which is determined by Grasshopper is used to identify if a design has a significantly reduced volume. If this design does not satisfy the following condition:

$$Volume \geq 0.9 * V_{target} \tag{9.1}$$

Where $Volume$ is the wetted volume of the vessel as determined by RhinoCeros and V_{target} is the target displacement which is the estimated displacement necessary to perform the stated function of the vessel. Then it is assumed that this design is unable to perform the required functions of the vessels. For this reason, this design will not be analysed using a CFD simulation to prevent the waste of computational time on infeasible designs.

9.1.2. Propeller power check

During testing, it was observed that despite the checks built into the parametric model on a rare occasion a design would get generated that passes all the built-in checks, but causes an error when STAR-CCM performs its meshing function. This results in a CFD simulation which has a required propeller power of 0. Because this is a result that HEEDS can interpret, this does not result in an error design. This would mean that without an artificial correction, the optimisation algorithm would interpret these designs as the optimal design instead of the error design it is. To correct this the following condition was implemented:

$$\begin{cases} P_{propeller.check} = P_{propeller} & \Leftarrow P_{propeller} \geq 10 \\ P_{propeller.check} = 10^8 & \Leftarrow P_{propeller} < 10 \end{cases} \tag{9.2}$$

This way when the algorithm is set to minimise the propeller power it will optimise away from these error designs

9.1.3. Displacement correction

A possibility to incorporate the displacement of the vessel in the optimisation would be to turn the optimisation study into a multi-objective study. However, both previous experience inside the organisation and the literature study showed that to achieve an optimised result for a multi-objective study more

design will need to be evaluated. Because of this a different method was chosen to incorporate the displacement of the vessel into the study while keeping the study single objective. For the first test run a displacement correction was implemented. To prevent the optimisation algorithm from optimising towards a vessel which has a smaller displacement than necessary to perform the stated purpose of the vessel. This correction was later replaced with a function which can alter the draft of the vessel, which is described in paragraph 11.1. The volume correction works according to the following function.

$$\begin{cases} P_{propeller.corrected} = P_{propeller} & \Leftarrow Volume > V_{target} \\ P_{propeller.corrected} = P_{propeller} * \left(1 + \frac{V_{target-Volume}}{V_{target}}\right)^{22} & \Leftarrow Volume \leq 100871 \end{cases} \tag{9.3}$$

In this equation, $P_{propeller}$ is the required propeller power as determined by the CFD simulation and $P_{propeller.corrected}$ is the required propeller power with the volume correction incorporated. This correction artificially increases the value of the propeller power for designs which have too little displacement which allows the algorithm to avoid these designs. This correction factor was determined to result in a required propeller power which is a factor of 100 larger than the required propeller power of the base design the the smallest possible Volume is analysed. When a design has a larger volume than the target displacement the required propeller power will not be corrected. This choice is made because the vessel is designed to transport transformer stations. Because of this, the operations of the vessel will not benefit from an increased displacement. The optimisation algorithm will have the stated goal of reducing this corrected propeller power.

III

Results

10

First test run

Before a larger optimisation study is performed a test run will first be performed, this test run has the goal of finding any previously unnoticed errors and eliminating them before a definite study is executed. For the optimisation algorithm, a population size of 8 is used as previously discussed. For the first test study, a population number of 5 is used. There is a chance that this does not result in enough iterations for the algorithm to make improvements. This does however allow for enough iterations to review the results before an eventual continuation of the study. For this test to be successful it needs to fulfill the following criteria.

- All the error designs must not have an impact on the study results
- The expected amount of designs are evaluated
- Any outlier designs which are included in the study results are caused by the shape of the design itself.
- For each design the input values are known, together with all output values necessary to evaluate the performance of each design
- The algorithm shows a trend towards a design with a lower required propeller power

The results of this first study can be found in the following figure 10.1, while a plot of the results excluding the outliers can be found in figure 10.2 and an overview of the results can be found in figure C.1: Some observations can be made from this data. Design 20 stands out since it has a significantly smaller required propeller power than the other designs. After some investigation, it was found out that this is caused by an error when creating the virtual towing tank which results in the model not being included as can be seen in figure 10.3. Extensive investigation has been done, but a cause for this error has not been found. To prevent this and similar designs from affecting the optimisation algorithm the condition for the propeller power will be increased to incorporate these designs. Furthermore, it has been noticed that the algorithm has not managed to test a design which performs better than the proposed design.

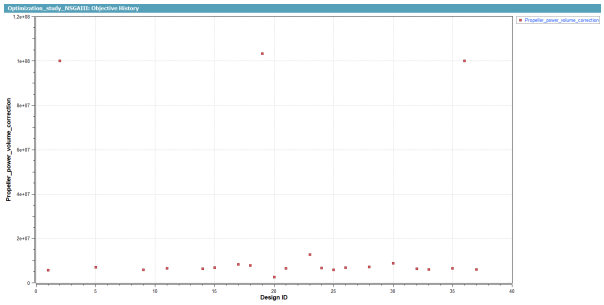

Figure 10.1: Plot of the results of the first test study

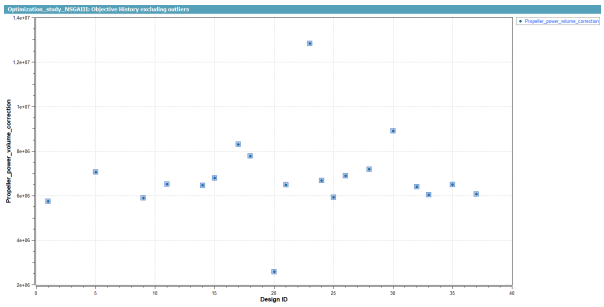

Figure 10.2: Plot of the first test results excluding the outliers

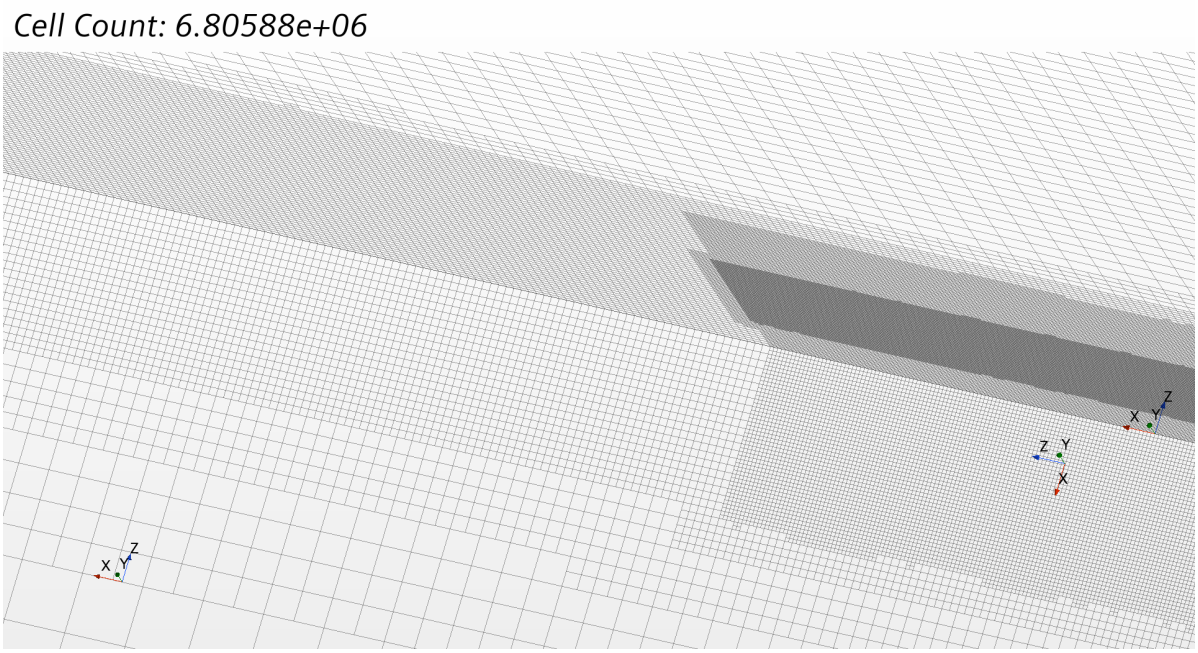

Figure 10.3: 3dimensional view of mesh from design 20

Although this is in the realm of expectations for a limited test some proposals were made to improve the results when performing a definitive study.

- It was observed that the performance value generated by HEEDS for the error designs is closer to the performance value for non-error designs than expected. For the start of the optimisation, this can cause the algorithm to incorporate these designs in its optimisation function. To prevent this the $P_{propeller.check}$ which was described in equation 9.2 will be increased to 10^{10}
- It is also possible that the volume correction which was described in equation 9.3 applies constraints which prevent the study from converging to a better design. To prevent this a different method was proposed to correct for the volume fluctuations: instead of adding a correction factor in the Propeller power function the depth of the design will be edited such that the volume of each design will be constant. This is found to be a better representation of the operation conditions of the proposed design. Taking the current results into account it is also expected that this will have a limited impact on the results since the variation in volume between the designs is limited.
- It was also observed that with the current set-up, it is not possible to separate the effect the design has on the propeller performance and the effect of the design on the total resistance. Evaluating these separately can give more insight into which factor of the improved design can be attributed to a reduction of the total resistance and which factor to the improvement of the propeller hull interactions. To be able to evaluate this effect a thrust deduction factor will be determined for each design. How the thrust reduction itself is determined is explained in equation 4.14. To be able to review the thrust deduction factor for each design the towing resistance of each design needs to be evaluated. To achieve this the effects of the virtual disks will be delayed in the CFD simulation until after the total ship resistance has converged thus allowing for the determining of the towing resistance without the need of running two simulations.

Besides these observations, the study satisfies the criteria for success which are stated above. Because the proposed differences will fundamentally change the results of the CFD simulation another test study will be performed

11

Second test run

This chapter will discuss the results of the second test run which was run after implementing the changes suggested in chapter 10. Of these changes, the suggestion to use a variable draft instead of applying a volume correction will be further elaborated upon. The vessel is designed to transport large converter stations, because of this the load the vessel will be required to carry will not change much over the lifetime of the vessel. Because of this changing the draft will simulate the case of the vessel carrying this load more accurately than applying an arbitrary volume correction.

11.1. Determining the required draft

In this section, it will be explained how the required draft is determined. First, a target displacement is determined, for this project this target displacement was already determined in an earlier design phase. With this target displacement, a function was added to the grasshopper model which evaluates the ship displacement at a range of drafts between 8.5m and 10.5m. This range was determined such that for all possible designs the required displacement will fall between the range of displacements which results from this range in drafts. The required draft is determined by performing a linear interpolation on the range of displacements. This results in a required draft which will be an input for STAR-CCM to perform the CFD analysis at the correct draft. As mentioned in chapter 10 the changes in the draft are expected to be small. Because of this, this change in the draft will also have a minimal effect on the waterplane area of the vessel. This will result in the expected effect of this change on the other hydrodynamic and hydrostatic properties of the vessel such as stability being minimal.

11.2. Results

With these changes, a second test was performed to make sure that no unexpected errors would occur when the larger study was executed. The results from this test are shown in figure 11.1 The values from the study can be found in figures C.2 and 11.2, where in figure 11.2 the two outlier design were excluded to allow a more detailed analysis of the other designs.

One possible error design can be observed, this is design number 16. The required power for this design is significantly larger than for other designs. This design corresponds with figure 11.3.

As can be seen in this figure this vessel design contains sharp angles which disturb the flow around the vessel and increase the pressure resistance around the hull. Because of this, the results are not caused by an error design, but by a sub-optimal design. Two general observations can be made about the performance of the NSGA-III algorithm. It can be observed that the NSGA-III algorithm after 28 designs converged to a group of designs which resulted in a comparable required power as the reference design. Design 36 is the first design which performs better than the base design. This improvement is smaller than the discretisation error and thus is not a significant improvement, however, this does show that the NSGA-III algorithm is capable of finding an improved solution with a small sample size. Based on the results from these two test studies it was decided to perform the following definite studies: One study will be performed using the NSGA-III algorithm with a population size of 8 for 10 generations. The choice for 10 generations was made based on the fact that experience inside

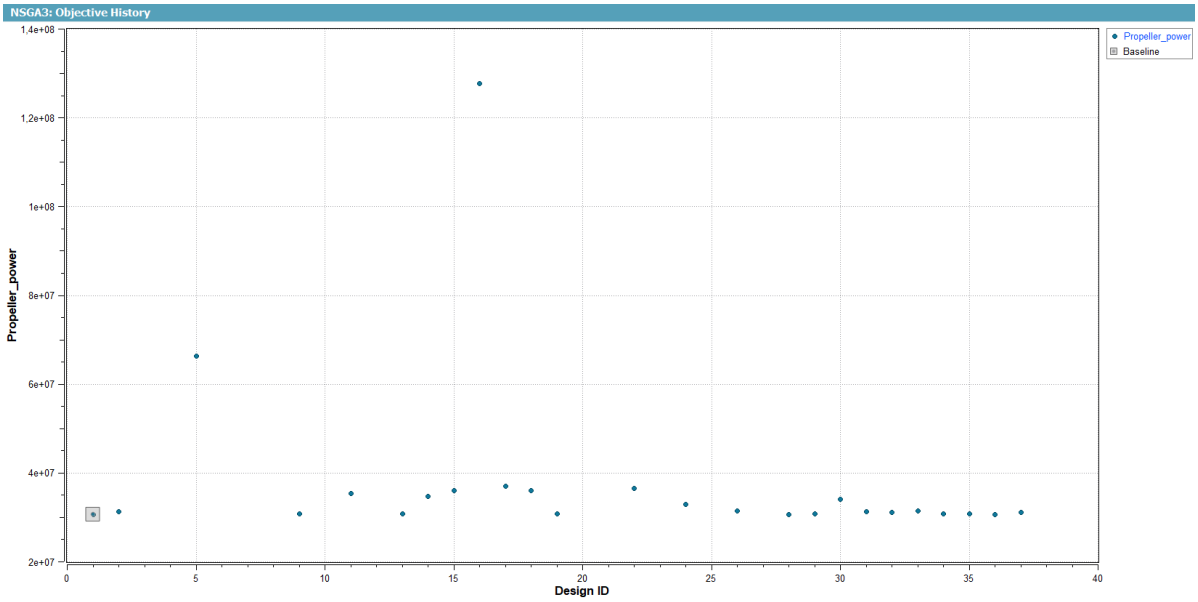

Figure 11.1: Objective history for the second NSGA-III test

Vuyk and the recommendations from Siemens show that for an optimisation study with 4 variables 80 designs should be a sufficient amount of evaluation to show improvement in the design objective. As a comparison a study will also be performed with the SHERPA algorithm of Siemens, this algorithm will also analyse 80 designs to make the comparison fair.

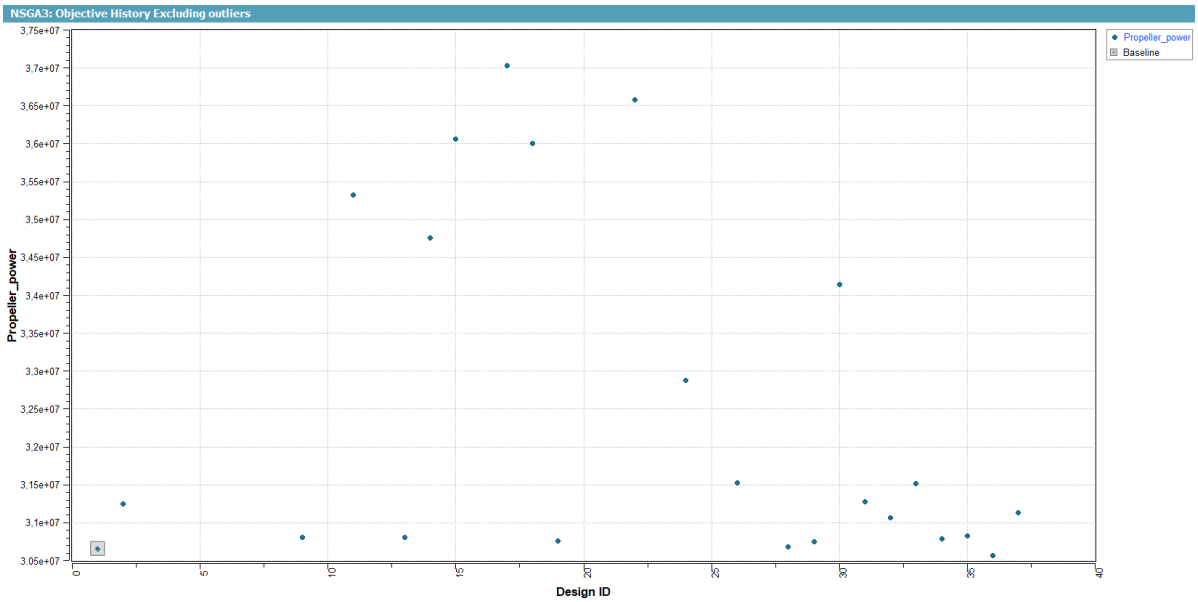

Figure 11.2: Objective history for the second NSGA-III test excluding outliers

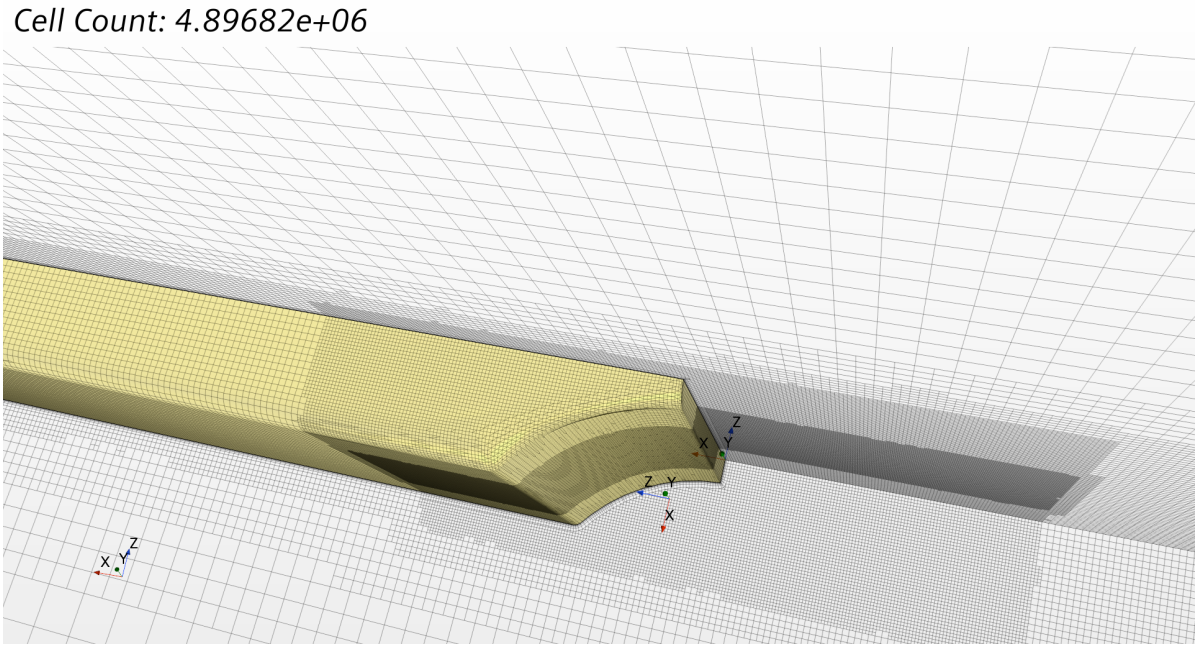

Figure 11.3: Aft-ship design 16

12

Final optimisation studies

In this chapter, the results from the definite studies will be discussed. As described in chapter 11 two studies were performed, one study using the NSGA-III algorithm with a population size of 8 and 10 generations and one using the SHERPA algorithm with the goal of analysing 80 designs.

12.1. NSGA-III study

In this section the results from the NSGA-III study will be discussed an overview of the objective history can be found in figure 12.1 while a table of all the variables can be found in figure C.3

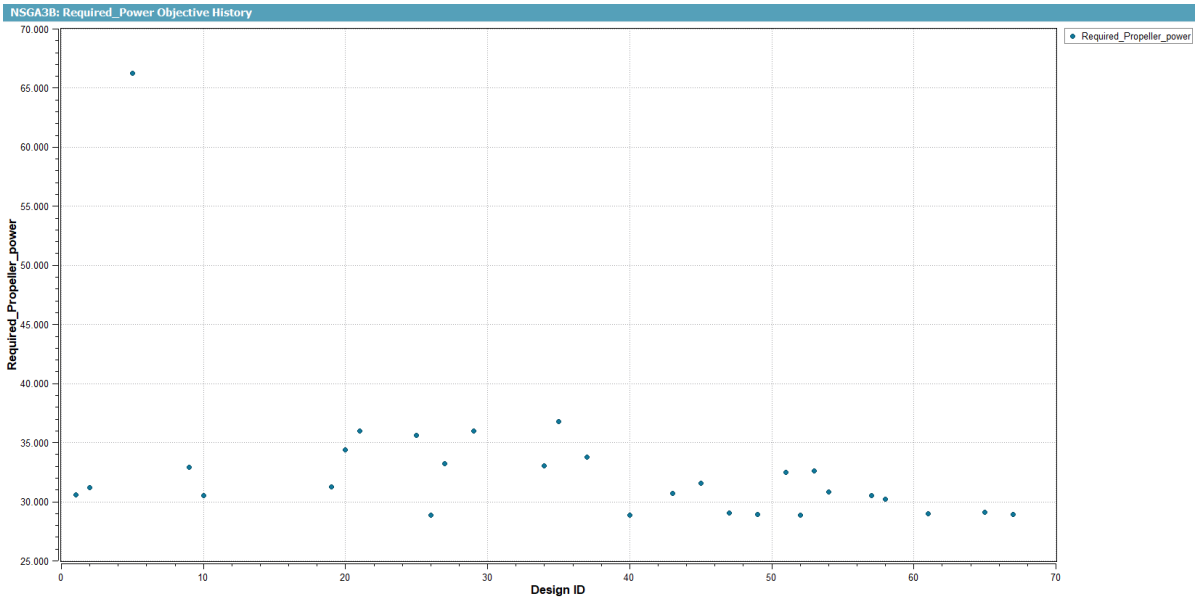

Figure 12.1: Objective history definitive NSGA-III study

One design stands out as a potential error design, this is design number 5 as illustrated in figure 12.2. This is a design with sharp edges and a large AftShipAngle, similar to design 16 of the test study, which was shown in figure 11.3. These design aspects are also an explanation for the high required propeller power which this design requires.

Figure 12.3 shows the objective history of the study excluding the outliers. As can be seen, the best design is design number 26. In the group of the final 30 designs, multiple designs have been evaluated which result in a required power which is close to the required power of design 26. It can also be noted that the total of designs which have been evaluated is not 80 because, after design number 26 the number of designs which will be evaluated in each population declined. This is caused by the sorting

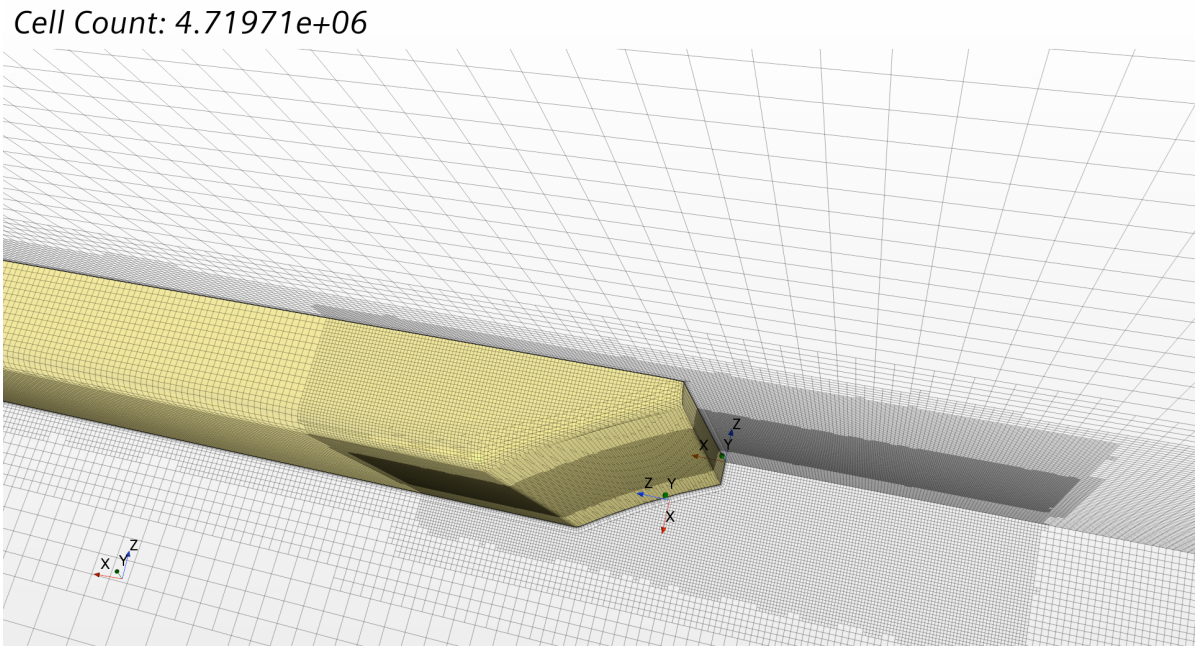

Figure 12.2: Design number 5

algorithm of NSGA-III which will include a dominant parent design in the next population however, since this simulation has already been analysed this solution will not be analysed again.

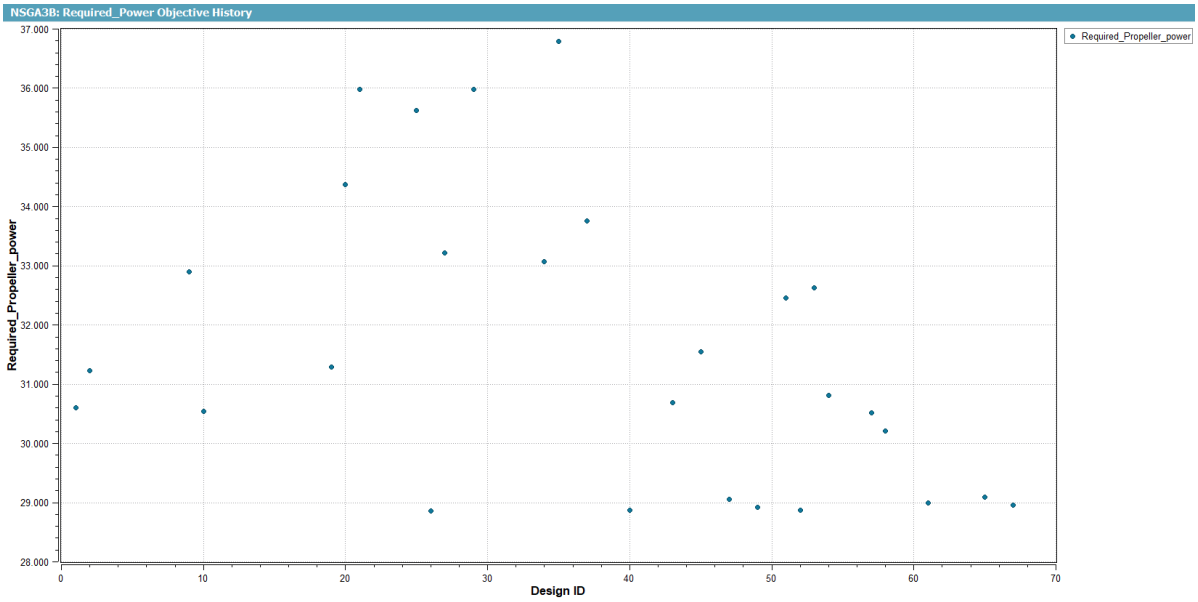

Figure 12.3: Objective history definitive NSGA-III study Excluding outliers

12.2. SHERPA study

As mentioned another test was performed making use of the SHERPA algorithm from Siemens, this comparison is made because SHERPA is the algorithm recommended by Siemens and most used by Vuyk Engineering for optimisation problems. Comparing these results to the results from the NSGA-III algorithm can give more insight into the efficiency of the algorithm even if the equations which the SHERPA algorithm uses are unknown. An overview of the results can be found in figure 12.4 while

the results themselves can be found in figures C.4 and C.5. Similar to the test study and the definitive

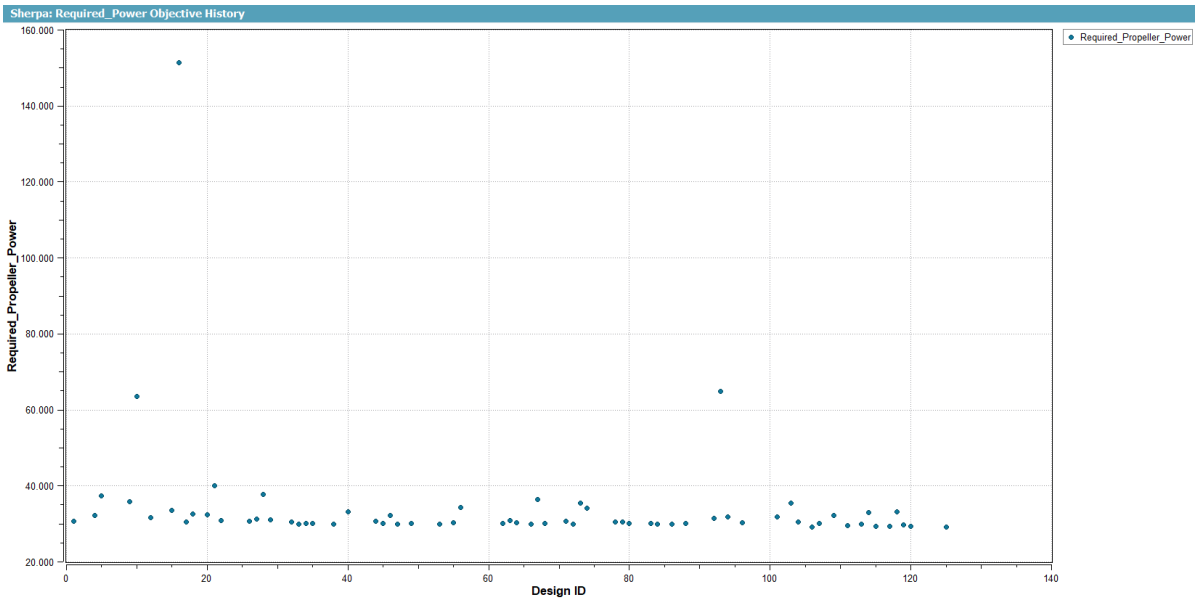

Figure 12.4: Objective history SHERPA study

NSGA-III study three outliers are found which will first be examined. These are designs 10, 16 and 93 an overview of which can be found in figure 12.5. As can be seen, all three of these designs are similar to design 16 of the test study, which is shown in figure 11.3. Because of this, the high required propeller power can also be explained by a similar phenomenon.

Figure 12.3 shows the objective history of the SHERPA study excluding the outliers. Since Siemens has not released a paper detailing the inner workings of the SHERPA algorithm an estimation will need to be made based on the results. In comparison to the previous study the SHERPA algorithm has been able to evaluate around 80 successful designs, this is caused by the flexibility of the SHERPA algorithm allowing an error design to be replaced by a new design which makes it possible to more accurately predict how many designs will be evaluated and thus how much computational resources will be used for this experiment.

12.3. Comparing algorithms

In figure 12.6 the objective histories of both the NSGA-III study and SHERPA study combined are shown. This allows for a comparison of both algorithms when performing an optimisation study for this vessel. To help with this comparison figures 12.7, 12.8, 12.9 and 12.10 show the history of the input parameters for both studies. Three things can be noted from this comparison. First, the NSGA-III algorithm needed less designs to arrive at a similar solution that the SHERPA had found. Also, the NSGA-III study converges after between 30 to 40 designs depending on the variables, while the SHERPA study does converge after 20 to 30 designs also depending on the variable, but to a lesser extent. Even when the SHERPA study converges it retains more diversity in the evaluated designs. The start of convergence of the NSGA-III study is most likely related to the evaluation of design 26 while the convergence of the SHERPA study is possibly related to the evaluation of designs 17 and 22 which are the first evaluated designs which have a similar performance number to the reference model. One reason why the SHERPA study needed more designs is the fact that the SHERPA study evaluated many designs with an Aft Arc Angle of 0. In comparison, the optimal design determined by the NSGA-III study has an Aft Arc Angle of 10 and the optimal design determined by the SHERPA study has an Aft Arc Angle of 8. A possible reason for this behaviour is the fact that a large input number for both the Aft Arc Angle and Aft Ship Angle will result in an error design. This might have caused the SHERPA algorithm to converge around a local optimum using an Aft Arc Angle of 0. The Sherpa algorithm showed this behaviour even though it maintained more variety in designs than the NSGA-III algorithm. This is a possible indication that the SHERPA algorithm is ill-suited for these kinds

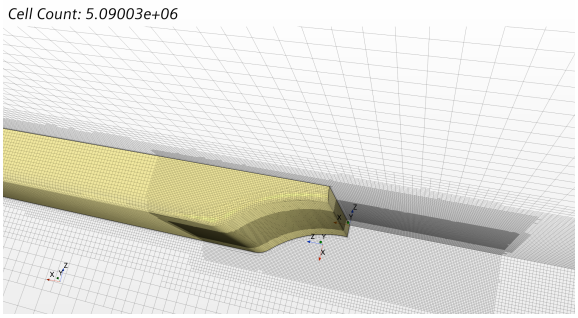

(a) Design 10

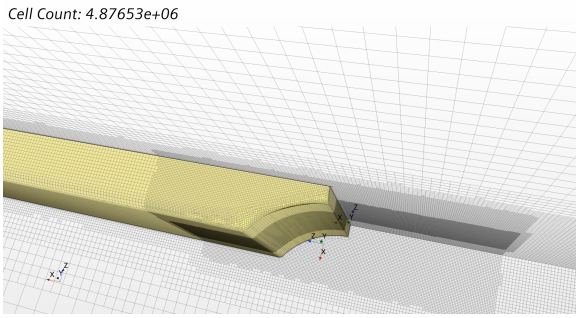

(b) Design 16

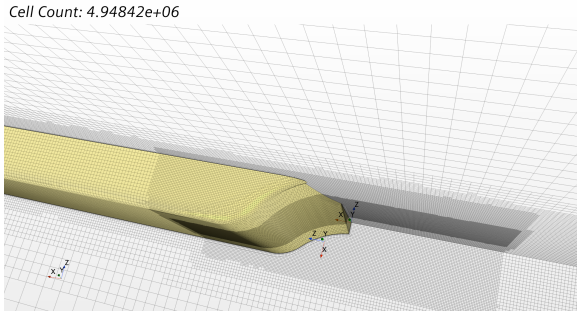

(c) Design 93

Figure 12.5: The aft ship of the SHERPA outlier designs

of optimization studies, where the limits are indicated by error design instead of limits on the input variables. Another possible reason why the SHERPA design performed worse is the fact that in this study the extreme design performed poorly. This might not work well with the method the SHERPA algorithm uses to maintain diversity. This one study does not provide enough information to indicate that in subsequent studies the NSGA-III algorithm can find a design similar to design number 26 in a comparable number of iterations. However, the fact that the NSGA-III study was able to find the right local optimum is an indicator that the NSGA-III algorithm is a better suited optimisation algorithm for this type of study.

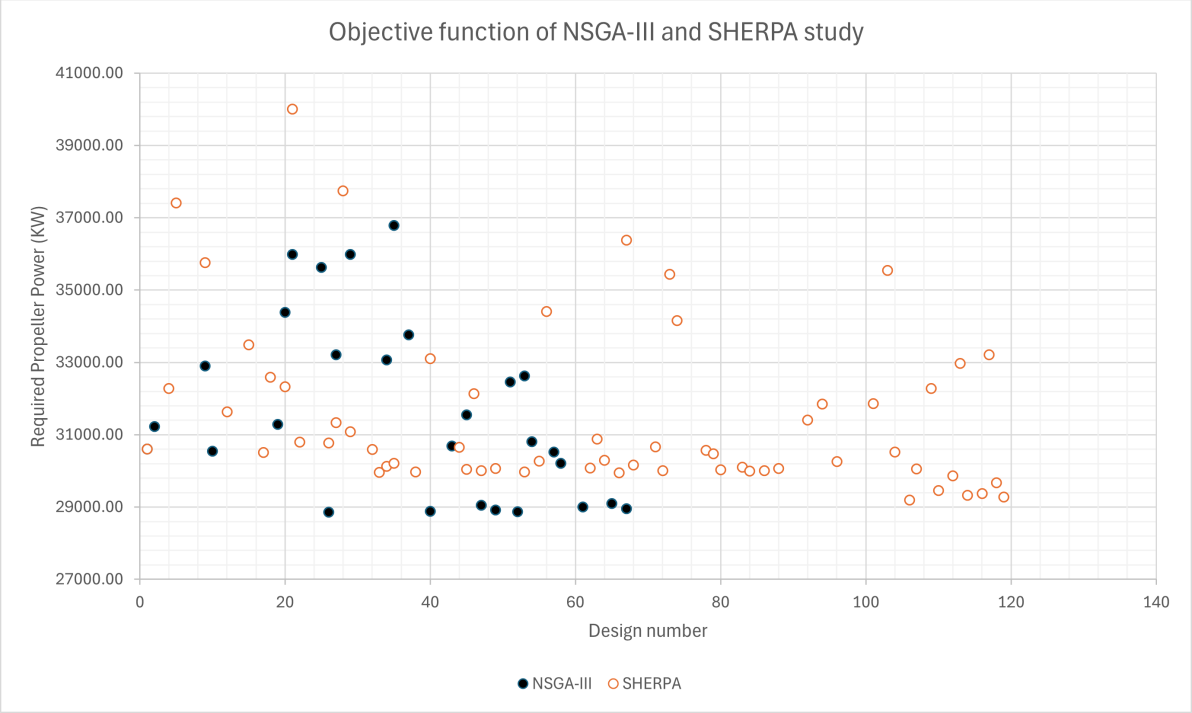

Figure 12.6: Objective History of NSGA-III study and SHERPA study combined excluding outliers

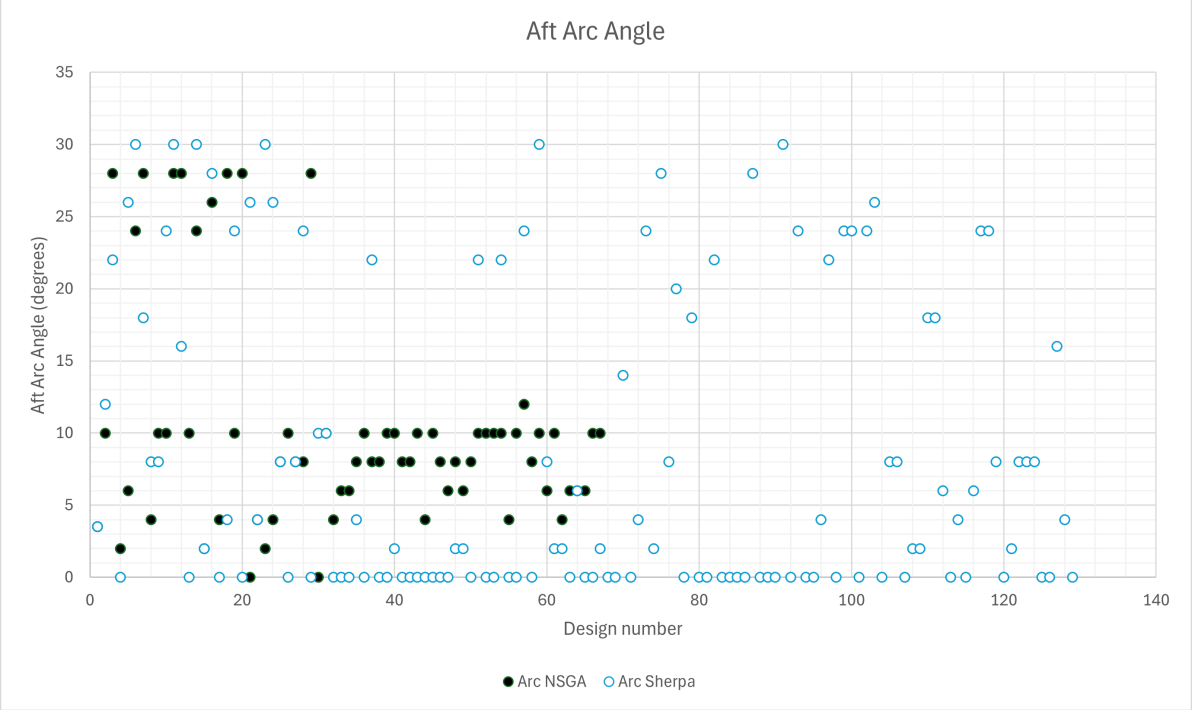

Figure 12.7: Aft Arc Angle

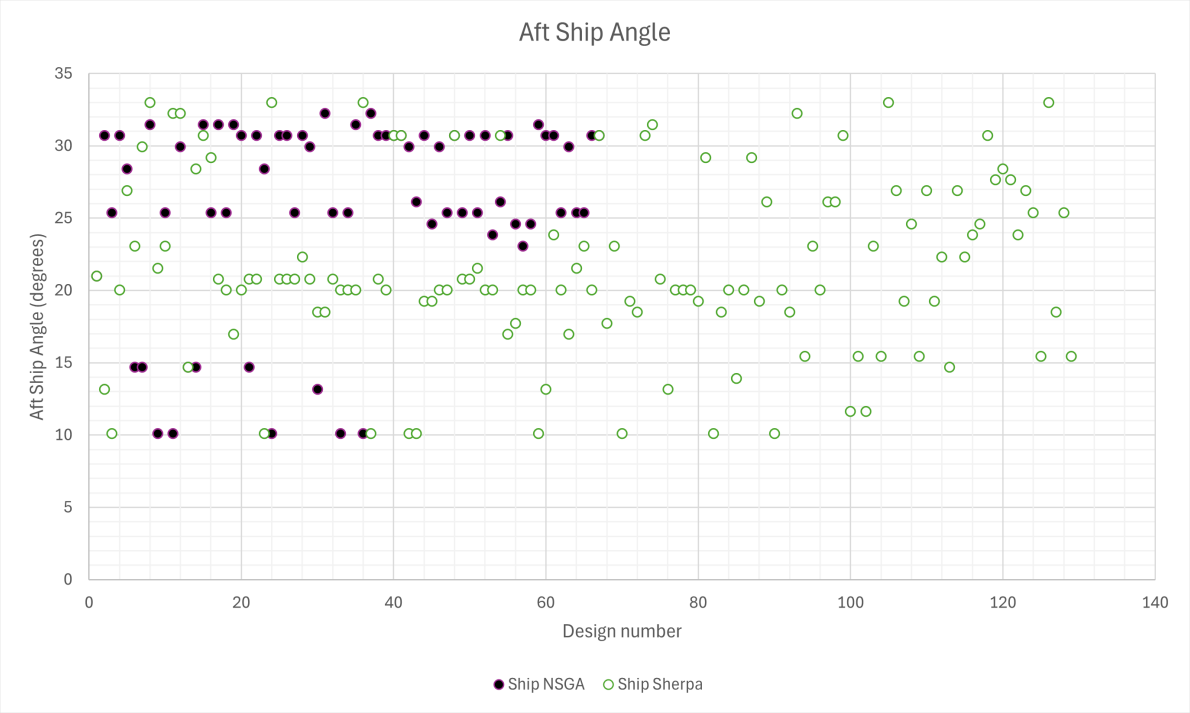

Figure 12.8: Aft Ship Angle

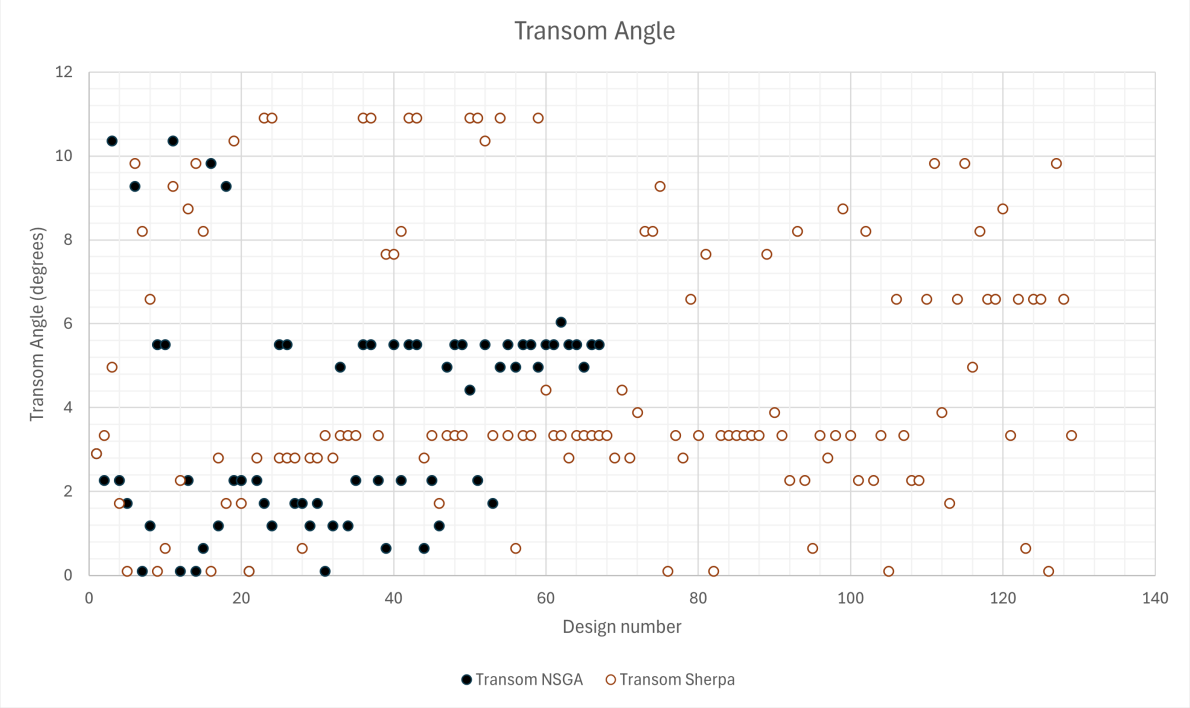

Figure 12.9: Transom Angle

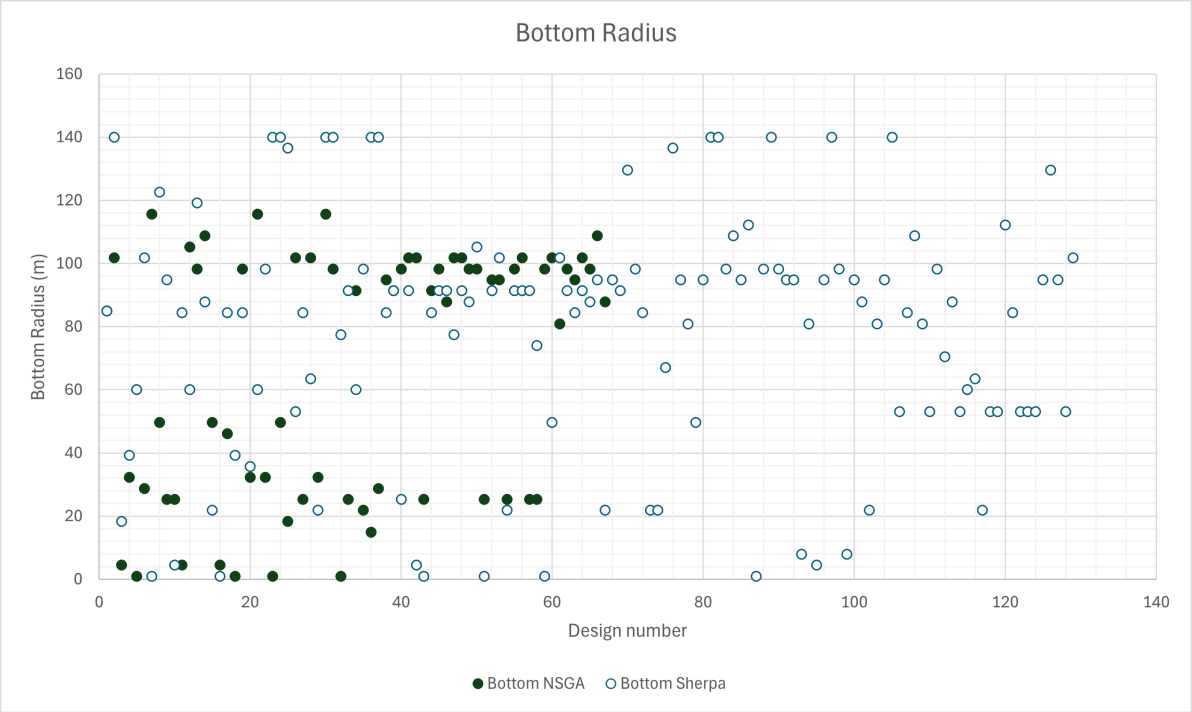

Figure 12.10: Bottom Radius

13

Validating the best designs

As mentioned in chapter 2 the best designs will be evaluated using a CFD analysis which includes the free surface effects to validate the assumption of leaving out the free surface effects in the simulation. The shape of the aft of the hull of these best designs can be found in figure 13.1. The results of the evaluations can be found in table 13.1.

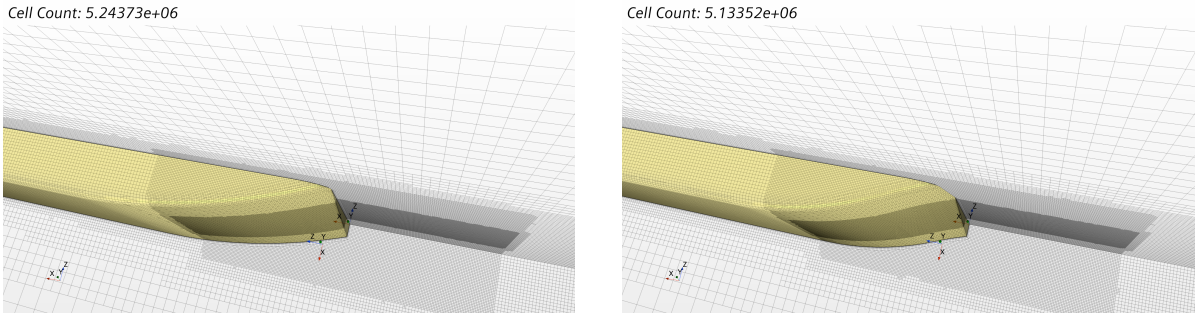

(a) Best Design of NSGA-III study

(b) Best design of the SHERPA study

Figure 13.1: Shape of the aft of the best design from both definite studies

Evaluation	Aft Arc Angle	Aft Ship Angle	Transom Angle	Bottom Radius	t (-)	w (-)	R_{shear} (KN)	$R_{pressure}$ (KN)	$P_{propeller}$ (KW)	Percentage of base
Base no free surface	10	25.37	5.5	25.325	0.11		227	136	3054	100%
Base free surface	10	25.37	5.5	25.325	0.036	0.10	224	171	2978	100%
NSGA-III no free surface	10	30.71	5.5	101.775	0.075		228	93.7	2886	94.29%
NSGA-III free surface	10	30.71	5.5	101.775	0.078	0.10	223	135	2660	89.31%
SHERPA no free surface	8	25.37	6.58	53.125	0.097		228	110	2914	95.21%
SHERPA free surface	8	25.37	6.58	53.125	0.107	0.13	225	140	2676	89.87%

Table 13.1: Results free surface evaluations of best designs

The required propeller power of the CFD analyses including the free surface is lower than the required propeller power of the analyses of the simulation excluding the free surface. Contrary to this the Pressure resistance for the analyses including the free surface is larger than those excluding the free surface. This is caused by an overestimation of the added wave-making resistance in the simulation which excludes the free surface. In addition to overestimating the wave-making resistance, the Holtrop

Mennen estimation of the wave-making resistance also underestimates the reduction in wave-making resistance caused by an improved design. Table 13.2 shows the relative difference in Propeller power between the analysis including the free surface and excluding the free surface. These differences

Analysis	Difference in $P_{propeller}$
Base	2.489%
NSGA-III	7.831%
SHERPA	8.168%

Table 13.2: Relative difference between analysis including and excluding the free surface

indicate that the exclusion of the free surface and the estimation of the wave-making resistance has introduced a significant margin of error in the optimisation study. The current studies do not provide enough information to be able to determine what impact this error in the estimation of the wave-making resistance will have on any further optimisation studies. For the currently run studies, it is not possible to know if a more accurate estimation of the wave-making resistance would have resulted in even better performing designs. However, the designs which were found with the current optimisation studies are a significant improvement on the initial base design. The improvement is even larger when a simulation including the wave-making resistance is performed. It can also be noted that the improvement in required propeller power is for a large part the result of reducing the total resistance experienced by the design. To give insight into what effect the different designs have on the working point of the propeller figures 13.2 and 13.3 show the working point of all the designs in the propeller curve of the chosen propeller. Figure 13.2 shows an overview of the open water curves, while figure 13.3 shows a zoomed in version of the same curves to provide a more detailed view. The propeller working point for the CFD simulations including free surface effects corresponds with similar advance ratios for the base design and the optimum design found by the SHERPA algorithm. From this, it can be concluded that the propeller for both simulations performs using a similar open water efficiency. The working point for the CFD simulations including the free surface, for the optimum design found by the NSGA-III algorithm corresponds to a higher advance ratio. This working point corresponds to a slightly lower open water efficiency.

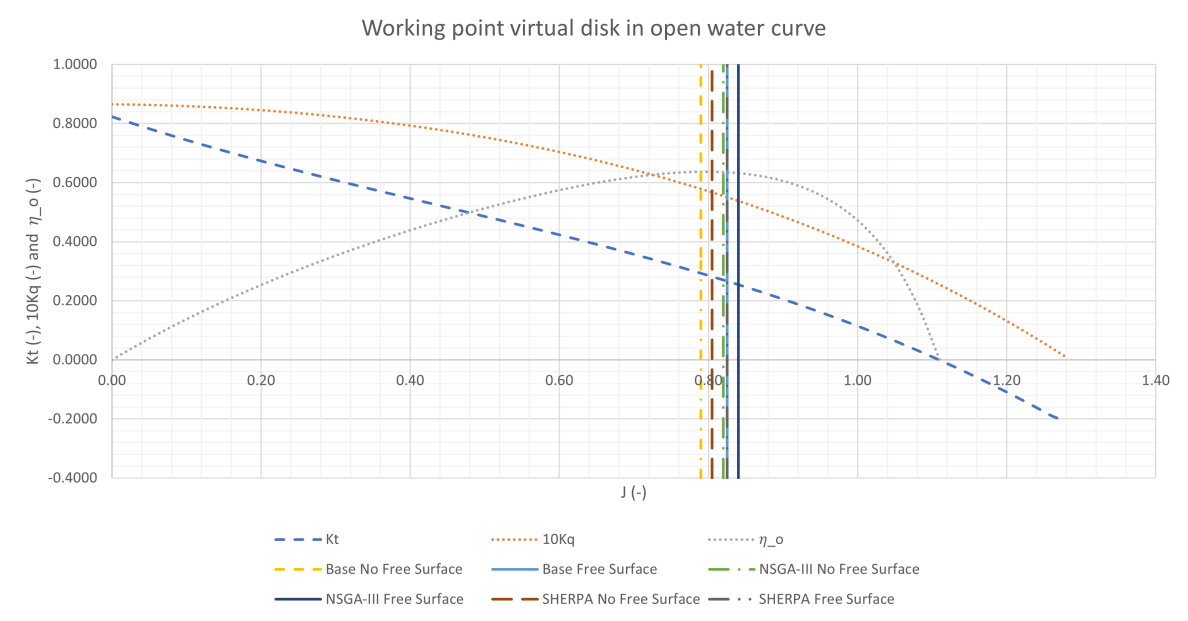

Figure 13.2: Working point of the propeller for the best and base designs

Table 13.3 shows an overview of the propeller efficiencies of the simulation including the free surface of the optimal designs. The hull efficiency η_H is determined using the following equation:

$$\eta_H = \frac{1-t}{1-w} \tag{13.1}$$

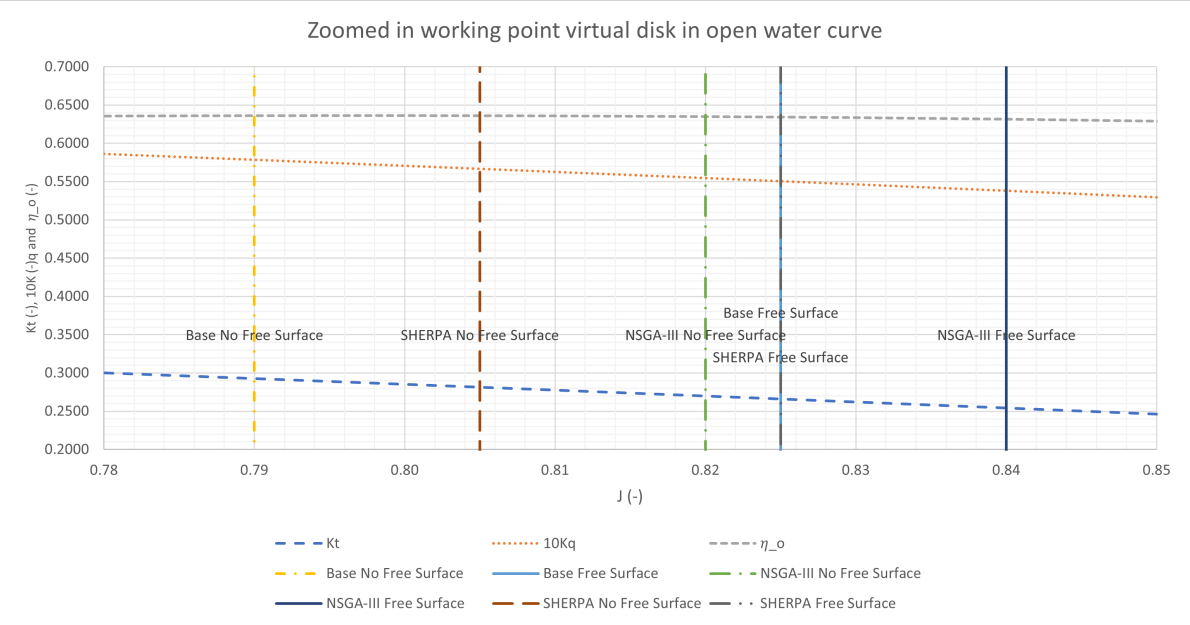

Figure 13.3: Working point of the propeller for the best and base designs zoomed in open water curve

Design	η_H	η_o	η_p
Base design	1.071	0.645	0.691
NSGA-III optimal design	1.024	0.64	0.656
SHERPA optimal design	1.037	0.645	0.669

Table 13.3: Propeller efficiency of the optimum designs

The open water efficiency η_o was determined using the open water curves and the relative rotative efficiency η_R is assumed to be 1. These efficiencies together form the propeller efficiency η_p. As can be seen, the propeller efficiency was lower for the optimized designs than for the base designs. The lower hull efficiency was the largest contributing factor to this phenomenon. This suggests that a trade-off has been made between the propeller-hull interaction and the resistance experienced by the vessel. The current study does however not give insight into what effect not including the propeller-hull effects would have on the optimisation result.

IV

Conclusions and recommendations

14

Conclusion

Building more fuel-efficient ships has always been a goal of shipbuilders, but with the recent IMO regulations, the main two examples being the EEDI and EEXI, this drive has increased further. One way to build more efficient ships is to design more efficient hull shapes. With the increase in computing power, this optimisation of the hull shape can increasingly be achieved with the help of Simulation-Based Design. The use of Computational Fluid Dynamics being one of the main use cases. The goal of this research is to develop and execute an optimisation strategy which can optimise the shape of the aftbody of a vessel to minimise the propeller power required for a vessel to sail at a constant speed. Which resulted in the following research questions:

- What geometrical parameters will need to be adjustable to be able to design the optimum aft shape?
- How can a CFD procedure be computationally light enough for an optimisation study using currently known techniques, while still being accurate and with enough resolution?
- How can the effects of a propeller be incorporated in an accurate way and with enough resolution into the CFD analysis while not adding as much computational load to make it unsuitable for an optimisation study?
- Which currently known optimisation method is the most effective and most efficient for this type of optimisation study?

This chapter will discuss the conclusions which can be drawn from the found answers to these research questions

14.1. Geometrical parameters

In this research the following four parameters were varied:

- Aft Arc Angle: Determines the angle at which the arc of the bottom from the transom is created.
- Aft Ship Angle: Determines the angle between the centre of the transom and the keel.
- Transom Angle: Determines the angle at which the transom rises to the side of the vessel.
- Bottom Radius: Determines the radius between the bottom and the rising aft of the vessel.

A more detailed explanation of these parameters can be found in chapter 5. These parameters have been shown to allow a large range of different aftbody shapes which have resulted in an approximately 10% reduction in the required propeller power. However, this study is not capable of determining if these parameters are the exact parameters which are capable of finding an optimum aft shape of the hull. In the recommendations, it will be discussed how a sensitivity study might be performed to find the exact relation the parameters have to the optimisation goal. From this study, it can only be concluded that using the discussed parameters an improved hullshape can be found.

14.2. Reducing computational load

This research has investigated multiple strategies to reduce the computational load of a single analysis: the choice was made to perform a RANS computation as opposed to both a BEM and an LES computation since literature research indicated that this type of computation contains the right balance between accurate results and computational load. A grid refinement study was performed to be able to estimate the discretisation error of different grid sizes. The choice was made to use a grid with a base cell size of 4.5 meters with refinements around the hull, the virtual disk and the wake of the vessel. This grid size corresponds with an uncertainty of 3.59%. This uncertainty is smaller than both the approximately 5% reduction in required propeller power achieved as indicated by the analysis without free surface included and the approximately 10% reduction in required propeller power achieved as indicated by the analysis with the free included. This indicates that a sufficiently fine grid has been used to investigate the difference between the different designs. The fact that the required propeller power was improved by 10% in the study including the free surface effects suggests that a coarser grid could also have been chosen, especially combined with an improved strategy for estimating the wave-making resistance.
Another strategy which has been used to reduce the computational time has been to replace the CFD analysis which included free surface effects with a CFD analysis which excludes free surface effects and estimates the wave-making resistance with the use of a Holtrop Mennen estimation. A comparison of the local velocities around the inflow of the virtual disk indicated that the inflow of the propeller would not be significantly impacted by excluding the free surface from the analysis. However, an investigation of the best designs shows that the estimation of the wave-making resistance using the Holtrop Mennen method is not accurate enough to be able to predict the working point of the propeller resulting in an overestimation of the required propeller power. This suggests that the strategy currently used for estimating the wave-making resistance does not provide accurate results. Not modelling the free surface effects does however save a significant amount of time, because of this in the recommendations possible improvements for this estimation will be discussed. Further research is needed to investigate if this estimation can be improved and what effect this estimation of the wave-making resistance has on the accuracy of the result.
The last strategy which has been used to reduce the computational load of the individual analyses is analysing only the aft half of the model while using the results from another analysis of the full vessel as an input for the local velocities halfway along the ship length. The CFD code is not able to compute the velocity difference between the input cells and the other cells in the mesh. This causes a computational error. Because of this, this strategy was not implemented in the final study. Because this strategy has not been successfully implemented it is also not possible to conclude if a significant improvement in computational time can be achieved using this strategy.

14.3. Incorporating the propeller

The effects of the propeller on the vessel are incorporated into the analysis using the virtual disk method. This method uses the open water curves of the Marin Ka 4-70 with nozzle 19a to estimate the effects of the propeller on the flow around the hull of the vessel. During the Literature research, two other methods of incorporating the propeller in the simulation were discussed. Simulating the propeller effects using the RANS method is the most computationally intensive method which has been investigated. A RANS-BEM hybrid model has also been investigated. In this method, the propeller effects are modelled using a BEM model. This model is less computationally intensive than the full RANS model. However, for an optimisation study for which the goal is to investigate as many designs as possible with a given amount of computational power and time while achieving accurate results with enough resolution, this model is still too computationally intensive. Because of this the Actuator disk method was used in this study.

14.4. Optimisation method

One of the criteria which were used to decide which optimisation algorithm to use is if the algorithm needed to run test studies to achieve settings which could provide the desired results. The theory behind this criterium is that it is preferable to run a larger definite study with a less efficient algorithm than to use a more efficient algorithm, but a smaller definite study because a part of the available computational resources was necessary to determine the correct input variables. Literature research

indicated that NSGA-III was the most effective open-source optimisation method which matched the criteria set beforehand. This method was compared to the SHERPA algorithm developed by Siemens. While both methods resulted in a comparable improvement in required propeller power the NSGA-III algorithm performed approximately half as many computations to achieve this result. Both algorithms require little knowledge and research into optimisation algorithms to be used effectively. Investigation of the results indicates that in a constrained study the SHERPA algorithm investigates designs around a local optimum which prevents the finding of the global optimum. For this reason for this specific study, it can be concluded that of the two algorithms tested the NSGA-III algorithm shows the most promising results.

14.5. Conclusion

The chosen set-up resulted in a significantly improved design, which supports the conclusion that the chosen set-up is capable of reducing the propeller power required for a heavy lift vessel to sail at a constant speed. However, the added uncertainty caused by the exclusion of the free surface from the analysis results in the fact that it is not possible to conclude that the current set-up can result in a significant improvement for different base models. To be able to draw this conclusion further research is needed in the exclusion and estimation of the free surface effects.

15

Recommendations

Some of the research questions could not be answered with a definite answer, while during this research new questions and topics came up which could be researched further. This chapter will discuss the different recommendations which are a result of the findings achieved in this study.

15.1. Input parameters

To be certain which parameters are the most effective when designing an optimum aft ship, a sensitivity study will need to be performed which will include more parameters than the current study. Two parameters which can be included in this sensitivity study on top of the parameters which were included in this study are the height of the transom and the length of the aft ship. To successfully perform this sensitivity study a broad range of designs will need to be investigated. This will allow for an accurate determination of the relation between the input parameters and the optimisation goal.

15.2. Computational load

To maintain accurate results while not increasing the computational load a better estimation of the wave-making resistance is needed. This could be achieved by using an improved correction factor which could also correct for the reduced wave-making resistance experienced by improved designs. Another strategy to improve the accuracy of the wave-making resistance estimation would be to make use of a different set of equations than the Holtrop Mennen estimation which are better suited for this type of vessel. When both these methods do not provide the desired results an optimisation strategy using CFD analyses which include the free surface will need to be investigated. When the accuracy of the results is improved using one of the suggested strategies making use of a coarser mesh could be investigated to save on computational time. Since the real achieved improvement is around 10% it could be possible to achieve a significantly improved result using a higher discretisation error.
Another strategy which was investigated is only modelling the aft half of the vessel. In this study, this strategy was not successful. A method could be developed to be able to transfer more hydrodynamical information from the study of the complete hull to the study of the partial hull. This way the inability to compute the sudden change in velocity could be resolved. Ramping up the input velocities to the velocities of the full simulation might also be a way to solve the current problem. When this strategy is implemented successfully the uncertainty this assumption introduces does need to be investigated

15.3. Simulating the propeller

For the current study modelling the propeller using the hybrid RANS-BEM method would be too computationally intensive. For a further study which has more computational power available simulating the propeller using this method could be investigated. On the other hand, the improvement from the currently run studies is for the most part a result of reducing the resistance experienced by the vessel. A further study could investigate what effect not modelling the propeller effects in the simulation will have on the optimisation study. If this optimisation study results in similar designs this might suggest

that a computationally lighter CFD simulation without modelling the propeller effects can achieve similar results and could thus be preferable.

15.4. Optimisation method

In the current study, a single study was run using the NSGA-III algorithm and a single study was run using the SHERPA algorithm. Both algorithms have proven to be capable of finding an improved design, with the NSGA-III algorithm finding this design faster than the SHERPA algorithm. However, to gain more insight into the efficiency of these algorithms a broader study will need to be performed with different hull shapes. Additional research can also be done into the use of different optimisation algorithms, for example, the NSGA-II algorithm and the Particle Swarm Optimisation algorithm. Additional research can also be done into different optimisation techniques, for example with the use of surrogate models or with the use of multi-fidelity optimisation techniques.

Appendices

A

Details grid refinemnt study

Grid type	Number of mesh elements	Base cell size	Relative step size	Propeller Power	Richardson error	Verification tool uncertainty
Grid 5	195815	18.02637	2.9996	3896952.622	14.37519713	24.91
Grid 4	405278	12.74657	2.3537	3578797.203	6.763143857	17.73
Grid 3	878275	9.013185	1.8188	3487102.972	4.311457755	9.89
Grid 2	2184750	6.373284	1.3424	3397874.372	1.798664844	5.41
Grid 1	5284651	4.506592	1	3361602.269	0.739060332	3.59
Richardson	-	0	0	3336758	0	-
Verification tool	-	0	0	3278300	-	0

Table A.1: Results grid refinement study

B

Example images

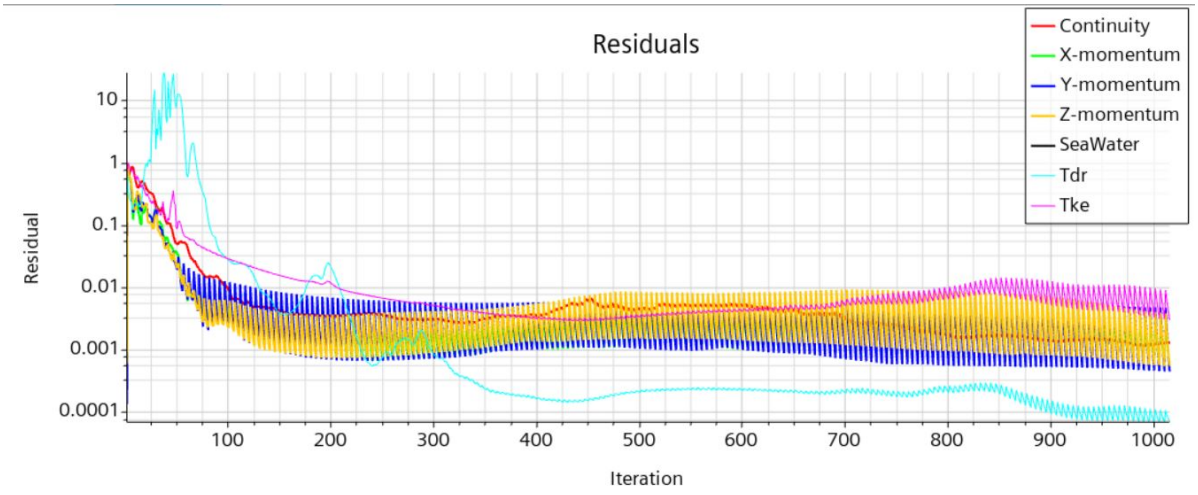

Figure B.1: CFD residuals

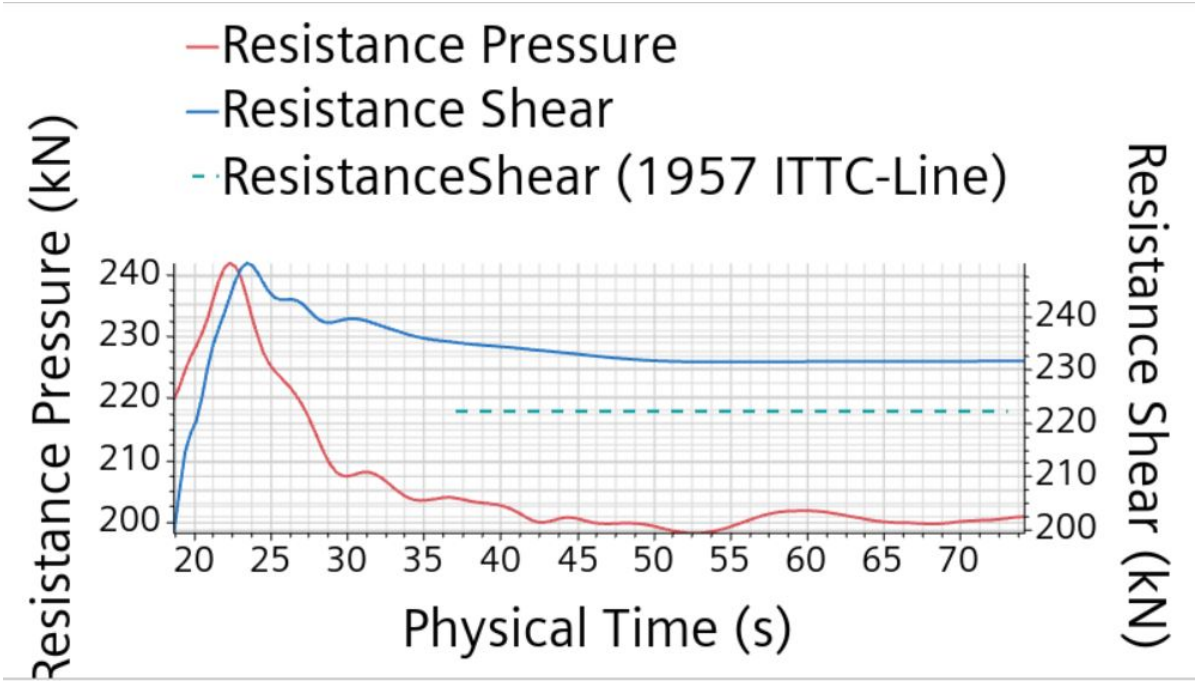

Figure B.2: Pressure and frictional resistance

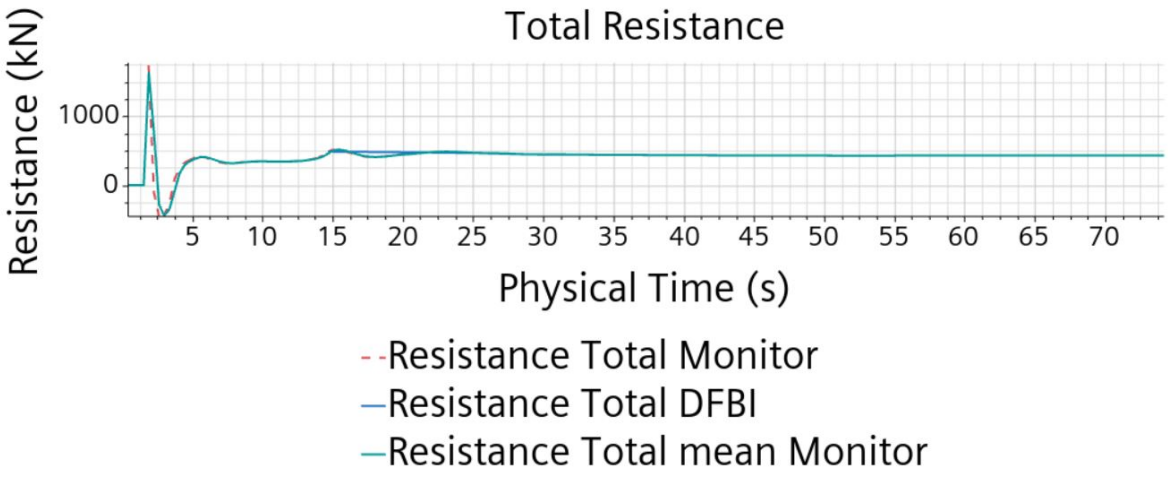

Figure B.3: Total resistance

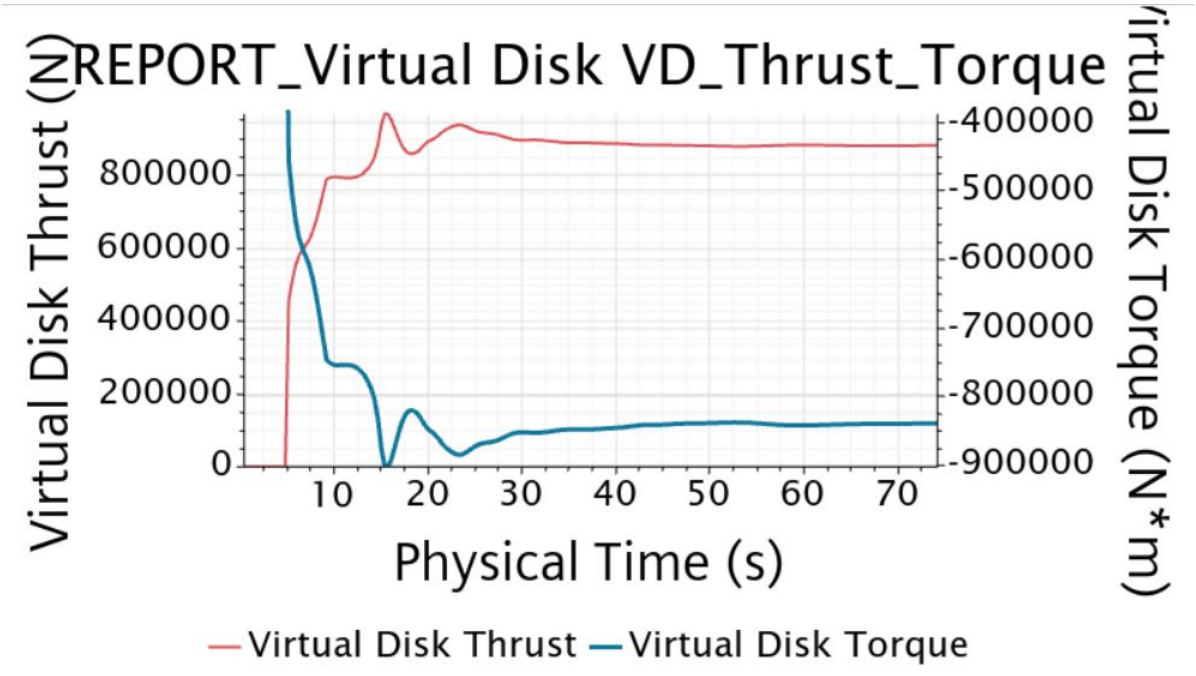

Figure B.4: Propeller thrust and torque

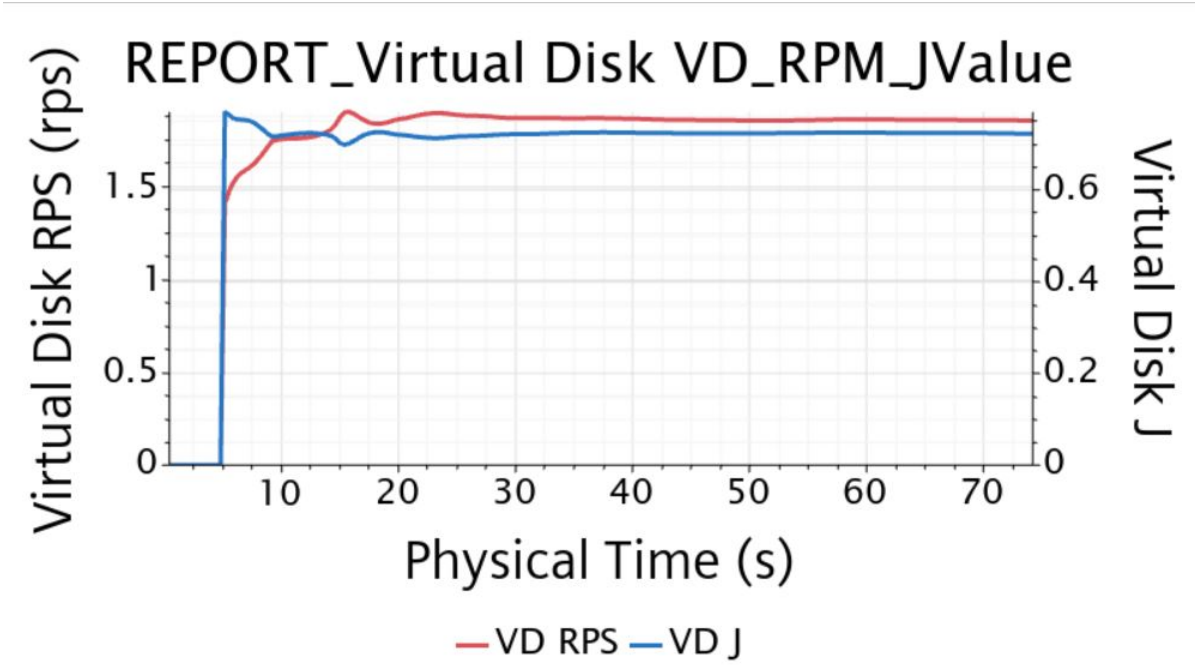

Figure B.5: Propeller rpm and J value

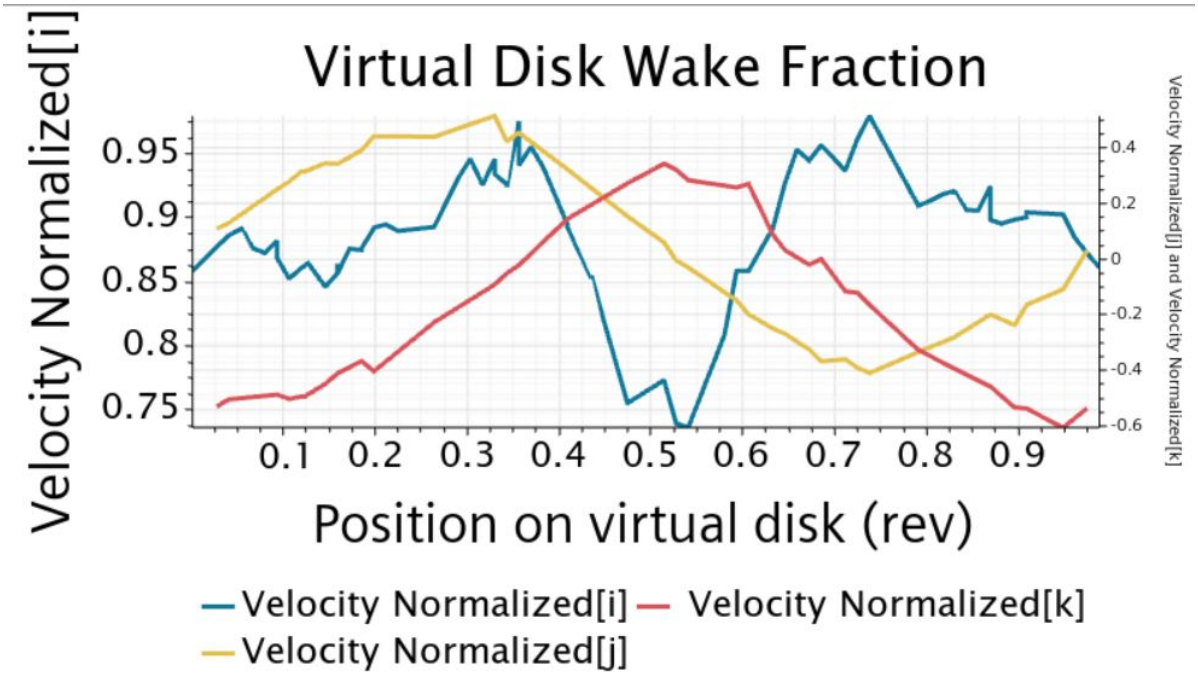

Figure B.6: Local velocity around edge virtual disk

C

Results optimisation studies

Design ID	performance	Propeller_power	Volume	Propeller_power_volume_correction	Aft_Arc_Angle	Aft_Ship_Angle	Transom_Angle	Bottom_Radius
1	-2	5,74601e+06	101022	5,74601e+06	4	21,25	3,1	85
2	-18,4034	0	101201	1e+08	9,23077	30,1696	2,31053	102,2
5	-2,22975	7,06618e+06	103455	7,06618e+06	6,92308	27,8393	1,75789	5
9	-2,02712	5,90187e+06	101081	5,90187e+06	4,61538	21,625	2,86316	86
11	-2,13465	6,51969e+06	102810	6,51969e+06	6,92308	23,9554	1,75789	5
14	-2,12448	6,46128e+06	102299	6,46128e+06	25,3846	30,1696	2,31053	32
15	-2,18254	6,7949e+06	100955	6,7949e+06	0	15,4107	0,1	118,4
17	-2,44623	6,79913e+06	99946,7	8,31002e+06	6,92308	15,4107	0,1	113
18	-2,35491	6,85865e+06	100288	7,78533e+06	6,92308	15,4107	0,1	80,6
19	-18,9874	0	100720	1,03356e+08	4,61538	22,4018	2,86316	107,6
20	-1,4498	2,42878e+06	100586	2,58458e+06	23,0769	30,1696	2,31053	102,2
21	-2,13004	6,49321e+06	103109	6,49321e+06	9,23077	30,1696	2,31053	32
23	-3,2335	1,28337e+07	102568	1,28337e+07	25,3846	27,0625	1,75789	5
24	-2,1628	6,68149e+06	103055	6,68149e+06	4,61538	23,9554	1,20526	5
25	-2,03165	5,92785e+06	101446	5,92785e+06	2,30769	21,625	2,31053	86
26	-2,19989	6,73625e+06	100764	6,89459e+06	0	14,6339	0,1	118,4
28	-2,2505	7,18541e+06	102869	7,18541e+06	25,3846	30,9464	0,1	32
30	-2,55132	6,3883e+06	99331,9	8,9139e+06	20,7692	21,625	2,31053	102,2
32	-2,11446	6,40371e+06	102123	6,40371e+06	6,92308	20,8482	1,75789	5
33	-2,05164	6,04273e+06	101636	6,04273e+06	4,61538	23,9554	2,31053	80,6
35	-2,1311	6,49934e+06	102007	6,49934e+06	9,23077	20,8482	1,20526	21,2
36	-18,4034	0	101221	1e+08	2,30769	21,625	2,31053	96,8
37	-2,05745	6,0761e+06	101036	6,0761e+06	20,7692	29,3929	2,31053	86

Figure C.1: Design table for the first optimisation test

NSGA3: Design Table

Design ID	Aft_Arc_Angle	Aft_Ship_Angle	Transom_Angle	Bottom_Radius	performance	Propeller_power	Thrust_deduction_	Draft	Wake_fraction	Resistance_shear	Resistance_pressu	Wave_resistance
1	3,5	21	2,9	85	-2	3,0656e+07	0,000176433	9,48	1,0458	228503	120011	633,298
2	10	30,71	2,26	101,775	-2,01919	3,12442e+07	0,000171093	9,47	1,05457	228910	124609	633,967
3	28	25,3667	10,36	4,475	-1e+99							
4	2	30,71	2,26	32,275	-1e+99			9,28				
5	6	28,42	1,72	1	-3,16146	6,62617e+07	0,00122121	9,27	1,0895	226552	603843	645,918
6	24	14,68	9,28	28,8	-1e+99							
7	28	14,68	0,1	115,675	-1e+99							
8	4	31,4733	1,18	49,65	-1e+99			9,31				
9	4	20,7867	2,8	84,4	-2,00507	3,08116e+07	0,000167362	9,48	1,04688	228439	121997	633,297
10	28	28,42	10,36	4,475	-1e+99							
11	6	24,6033	1,72	1	-2,15231	3,53252e+07	0,000328031	9,32	1,00994	228718	210464	643,157
12	2	29,9467	2,26	21,85	-1e+99			9,27				
13	4	20,7867	2,8	80,925	-2,00503	3,08102e+07	0,000173701	9,48	1,04599	228529	122390	633,296
14	24	30,71	2,26	25,325	-2,13379	3,47576e+07	0,000327893	9,35	1,00979	227747	202573	642,17
15	0	14,68	0,1	115,675	-2,17631	3,6061e+07	0,000150001	9,51	1,09101	228789	181523	631,323
16	26	28,42	1,18	1	-5,16755	1,2776e+08	0,00180813	9,32	1,13174	221270	1,30401e+06	641,376
17	6	14,68	0,1	112,2	-2,2078	3,70263e+07	0,000101732	9,59	1,10259	227745	191723	626,117
18	0	14,68	0,1	80,925	-2,17448	3,60049e+07	0,000159437	9,4825	1,08762	228902	182124	633,155
19	4	21,55	2,8	112,2	-2,00346	3,07621e+07	0,000152018	9,5225	1,05683	228236	116833	630,5
20	24	14,68	2,26	112,2	-1e+99							
21	4	30,71	0,1	25,325	-1e+99			9,2392				
22	4	14,68	0,1	112,2	-2,19309	3,65754e+07	0,000134205	9,5589	1,10026	228171	185489	628,117
23	10	25,3667	10,36	4,475	-1e+99							
24	26	29,9467	2,26	94,825	-2,07249	3,28784e+07	0,000176633	9,5261	1,05455	227809	151920	630,237
25	6	24,6033	0,64	1	-1e+99			9,2994				
26	4	20,7867	2,26	84,4	-2,0284	3,15267e+07	0,000177285	9,4691	1,0507	228750	131167	634,026
27	22	30,71	2,26	21,85	-1e+99							
28	2	20,0233	2,8	77,45	-2,00083	3,06814e+07	0,000175887	9,4687	1,04459	228603	120877	634,054
29	4	21,55	2,8	115,675	-2,00301	3,07484e+07	0,000147504	9,5289	1,05825	228233	115957	630,079
30	24	29,9467	1,18	80,925	-2,11374	3,4143e+07	0,000202173	9,4595	1,05401	228565	170754	634,741
31	10	29,9467	2,26	101,775	-2,02035	3,12798e+07	0,000172978	9,4712	1,05465	228869	125202	633,887
32	4	19,26	2,8	80,925	-2,0133	3,10637e+07	0,00016465	9,504	1,05209	228285	123774	631,697
33	4	20,7867	2,26	80,925	-2,028	3,15143e+07	0,000177039	9,4639	1,04878	228673	132042	634,376
34	2	19,26	2,8	80,925	-2,00425	3,07863e+07	0,000162731	9,4856	1,0485	228452	120817	632,922
35	4	20,7867	2,8	77,45	-2,00544	3,08227e+07	0,000173549	9,4736	1,04522	228552	122913	633,725
36	0	21,55	2,8	84,4	-1,99719	3,057e+07	0,000192678	9,4476	1,04152	228884	120185	635,48
37	4	18,4967	2,8	73,975	-2,01557	3,11333e+07	0,000154354	9,511	1,05284	228128	124751	631,233

Figure C.2: Results second NSGA test

NSGA3B: Design Table

Design ID	performance	Aft_Arc_Angle	Aft_Ship_Angle	Transom_Angle	Bottom_Radius	Draft	Required_Propeller_	Thrust_deduction_	Shear_resistance	Pressure_resistanc	Wave_Making_Res	PropPowerRatio
1	-2	3,5	21	2,9	85	9,481	30603,1	0,0770076	228,501	119,317	61423,4	100
2	-2,02031	10	30,71	2,26	101,775	9,4699	31224,8	0,0752018	228,908	124,385	61495,5	102,031
3	-1e+99	28	25,3667	10,36	4,475							
4	-1e+99	2	30,71	2,26	32,275	9,2782						
5	-3,16471	6	28,42	1,72	1	9,2693	66246,9	0,364777	226,589	602,513	62659	216,471
6	-1e+99	24	14,68	9,28	28,8							
7	-1e+99	28	14,68	0,1	115,675							
8	-1e+99	4	31,4733	1,18	49,65	9,3053						
9	-2,07504	10	10,1	5,5	25,325	9,4841	32899,6	0,093488	230,108	159,623	59087,7	107,504
10	-1,99807	10	25,3667	5,5	25,325	9,4233	30544,2	0,111766	227,366	135,989	61770,8	99,8075
11	-1e+99	28	10,1	10,36	4,475							
12	-1e+99	28	29,9467	0,1	105,25							
13	-1e+99	10	14,68	2,26	98,3							
14	-1e+99	24	14,68	0,1	108,725							
15	-1e+99	2	31,4733	0,64	49,65	9,2932						
16	-1e+99	26	25,3667	9,82	4,475							
17	-1e+99	4	31,4733	1,18	46,175	9,2963						
18	-1e+99	28	25,3667	9,28	1							
19	-2,02235	10	31,4733	2,26	98,3	9,4609	31287,2	0,0782243	228,918	126,396	61554,2	102,235
20	-2,12336	28	30,71	2,26	32,275	9,3841	34378,3	0,114112	227,62	191,706	62064,9	112,336
21	-2,1759	0	14,68	0,1	115,675	9,5058	35986,3	0,0596766	228,778	180,712	61265,3	117,59
22	-1e+99	4	30,71	2,26	32,275	9,2855						
23	-1e+99	2	28,42	1,72	1	9,2573						
24	-1e+99	4	10,1	1,18	49,65							
25	-2,16415	8	30,71	5,5	18,375	9,329	35626,6	0,191071	227,681	222,608	62374,5	116,415
26	-1,94292	10	30,71	5,5	101,775	9,5583	28856,4	0,0747417	227,502	93,7015	60931,2	94,2924
27	-2,0854	8	25,3667	1,72	25,325	9,3351	33216,5	0,131526	228,389	176,26	62396,8	108,54
28	-1e+99	8	30,71	1,72	101,775							
29	-2,17582	28	29,9467	1,18	32,275	9,3731	35983,7	0,113158	227,852	212,466	62139,3	117,582
30	-1e+99	0	13,1533	1,72	115,675							
31	-1e+99	10	32,2367	0,1	98,3							
32	-1e+99	4	25,3667	1,18	1	9,2912						
33	-1e+99	6	10,1	4,96	25,325							
34	-2,08057	6	25,3667	1,18	91,35	9,4267	33068,9	0,0868379	229,266	152,106	61779,4	108,057
35	-2,20207	8	31,4733	2,26	21,85	9,274	36787,3	0,234892	229,154	254,339	62812,3	120,207
36	-1e+99	10	10,1	5,5	14,9							
37	-2,10312	8	32,2367	5,5	28,8	9,336	33759	0,177141	227,83	192,645	62377,5	110,312
38	-1e+99	8	30,71	2,26	94,825							
39	-1e+99	10	30,71	0,64	91,35	9,4089						
40	-1,9436	10	30,71	5,5	98,3	9,5485	28877,1	0,0775799	227,574	94,9312	60992,9	94,36
41	-1e+99	8	30,71	2,26	101,775							
42	-1e+99	8	29,9467	5,5	101,775							
43	-2,00285	10	26,13	5,5	25,325	9,4107	30690,4	0,118332	227,376	139,514	61848,1	100,285
44	-1e+99	4	30,71	0,64	91,35							
45	-2,03089	10	24,6033	2,26	98,3	9,4917	31548,5	0,074484	228,498	130,358	61360,5	103,089
46	-1e+99	8	29,9467	1,18	87,875	9,4111						
47	-1,94937	6	25,3667	4,96	101,775	9,55	29053,7	0,0723224	227,619	96,5397	60983,2	94,937
48	-1e+99	8	30,71	5,5	101,775							
49	-1,94491	6	25,3667	5,5	98,3	9,5578	28917,3	0,0763299	227,418	95,6143	60934,3	94,4913
50	-1e+99	8	30,71	4,42	98,3							
51	-2,06073	10	25,3667	2,26	25,325	9,3554	32461,6	0,118558	228,028	164,49	62247,7	106,073
52	-1,94341	10	30,71	5,5	94,825	9,5387	28871,4	0,0768324	227,658	95,6825	61054,8	94,3415
53	-2,06611	10	23,84	1,72	94,825	9,4783	32626,4	0,0755694	228,7	145,061	61443,1	106,611
54	-2,00666	10	26,13	4,96	25,325	9,3993	30807	0,116074	227,446	141,678	61925,4	100,666
55	-1e+99	4	30,71	5,5	98,3							
56	-1e+99	10	24,6033	4,96	101,775							
57	-1,99716	12	23,0767	5,5	25,325	9,478	30516,4	0,0935625	228,046	131,076	61438,6	99,7165
58	-1,98728	8	24,6033	5,5	25,325	9,4266	30213,8	0,105905	228,388	130,028	61765,3	98,7277
59	-1e+99	10	31,4733	4,96	98,3							
60	-1e+99	6	30,71	5,5	101,775							
61	-1,9476	10	30,71	5,5	80,925	9,4994	28999,4	0,0833408	227,959	100,442	61305,5	94,7595
62	-1e+99	4	25,3667	6,04	98,3							
63	-1e+99	6	29,9467	5,5	94,825							
64	-1e+99	6	25,3667	5,5	101,775							
65	-1,95074	6	25,3667	4,96	98,3	9,5416	29095,7	0,0750273	227,679	97,826	61036,2	95,0744
66	-1e+99	10	30,71	5,5	108,725							
67	-1,9462	10	30,71	5,5	87,875	9,519	28956,6	0,0815976	227,781	98,1739	61180	94,6198

Figure C.3: Results NSGA study

Sherpa: Design Table

Design ID	performance	Aft_Arc_Angle	Aft_Ship_Angle	Transom_Angle	Bottom_Radius	Draft	Required_Propeller_	Thrust_deduction_	Shear_resistance	Pressure_resistanc	Wave_Making_Res	PropPowerRatio	P
1	-1	3,5	21	2,9	85	9,481	30603,1	0,0770076	228,501	119,317	61423,4	100	3
2	-1e+99	12	13,1533	3,34	140								
3	-1e+99	22	10,1	4,96	18,375								
4	-1,05478	0	20,0233	1,72	39,225	9,3845	32279,6	0,0976712	228,269	150,244	62062,1	105,478	3
5	-1,22244	26	26,8933	0,1	60,075	9,4399	37410,4	0,0846504	228,501	219,02	61692,2	122,244	3
6	-1e+99	30	23,0767	9,82	101,775								
7	-1e+99	18	29,9467	8,2	1								
8	-1e+99	8	33	6,58	122,625								
9	-1,16859	8	21,55	0,1	94,825	9,4476	35762,6	0,0768209	229,161	185,345	61644,1	116,859	3
10	-2,07942	24	23,0767	0,64	4,475	9,4079	63636,7	0,220669	224,738	584,98	61734,2	207,942	6
11	-1e+99	30	32,2367	9,28	84,4								
12	-1,0337	16	32,2367	2,26	60,075	9,3853	31634,5	0,109906	228,145	145,371	62056,6	103,37	3
13	-1e+99	0	14,68	8,74	119,15								
14	-1e+99	30	28,42	9,82	87,875								
15	-1,09408	2	30,71	8,2	21,85	9,3638	33482,4	0,158035	226,899	185,446	62163,8	109,408	3
16	-4,94484	28	29,1833	0,1	1	9,3012	151327	0,271908	221,892	1508,43	62392,4	494,484	1
17	-0,997011	0	20,7867	2,8	84,4	9,4542	30511,7	0,0822728	228,781	119,234	61598,2	99,7011	3
18	-1,06477	4	20,0233	1,72	39,225	9,4135	32585,3	0,0868643	228,184	151,435	61867,5	106,477	3
19	-1e+99	24	16,97	10,36	84,4								
20	-1,05623	0	20,0233	1,72	35,75	9,3822	32323,9	0,0983494	228,297	151,189	62077,7	105,623	3
21	-1,30708	26	20,7867	0,1	60,075	9,5608	40000,8	0,0557215	226,888	247,872	60913,4	130,708	4
22	-1,00648	4	20,7867	2,8	98,3	9,5061	30801,4	0,0709229	228,312	119,552	61267,7	100,648	3
23	-1e+99	30	10,1	10,9	140								
24	-1e+99	26	33	10,9	140								
25	-1e+99	8	20,7867	2,8	136,525								
26	-1,00555	0	20,7867	2,8	53,125	9,411	30772,9	0,098014	227,977	129,47	61884,1	100,555	3
27	-1,02406	8	20,7867	2,8	84,4	9,5173	31339,6	0,0720443	228,075	128,227	61189,4	102,406	3
28	-1,2334	24	22,3133	0,64	63,55	9,5263	37746	0,0646566	227,471	218,694	61131,8	123,34	3
29	-1,01584	0	20,7867	2,8	21,85	9,3874	31087,8	0,0994955	228,121	136,745	62042,7	101,584	3
30	-1e+99	10	18,4967	2,8	140								
31	-1e+99	10	18,4967	3,34	140								
32	-0,999765	0	20,7867	2,8	77,45	9,4428	30596	0,0858787	228,834	122,064	61673,1	99,9765	3
33	-0,979017	0	20,0233	3,34	91,35	9,4887	29961	0,0767283	228,436	109,69	61373,8	97,9017	2
34	-0,984374	0	20,0233	3,34	60,075	9,4455	30124,9	0,0872712	228,661	116,977	61655,3	98,4374	3
35	-0,987142	4	20,0233	3,34	98,3	9,5324	30209,6	0,0697896	227,977	111,399	61099,7	98,7142	3
36	-1e+99	0	33	10,9	140								
37	-1e+99	22	10,1	10,9	140								
38	-0,979465	0	20,7867	3,34	84,4	9,4687	29974,7	0,0800471	228,57	111,739	61503,6	97,9465	2
39	-1e+99	0	20,0233	7,66	91,35								
40	-1,08161	2	30,71	7,66	25,325	9,36	33100,6	0,158872	227,13	180,488	62192,8	108,161	3
41	-1e+99	0	30,71	8,2	91,35								
42	-1e+99	0	10,1	10,9	4,475								
43	-1e+99	0	10,1	10,9	1								
44	-1,00141	0	19,26	2,8	84,4	9,4724	30646,3	0,0785496	228,63	119,372	61479,2	100,141	3
45	-0,981742	0	19,26	3,34	91,35	9,4981	30044,4	0,0730117	228,322	110,381	61319,4	98,1742	3
46	-1,05006	0	20,0233	1,72	91,35	9,4444	32135,1	0,0807395	229,096	139,45	61662,4	105,006	3
47	-0,980418	0	20,0233	3,34	77,45	9,4673	30003,9	0,0818027	228,54	112,694	61512,6	98,0418	3
48	-1e+99	2	30,71	3,34	91,35								
49	-0,98257	2	20,7867	3,34	87,875	9,4892	30069,7	0,076103	228,385	111,855	61370,5	98,257	3
50	-1e+99	0	20,7867	10,9	105,25								
51	-1e+99	22	21,55	10,9	1								
52	-1e+99	0	20,0233	10,36	91,35								
53	-0,979486	0	20,0233	3,34	101,775	9,5071	29975,4	0,0701545	228,305	107,731	61255,4	97,9486	2
54	-1e+99	22	30,71	10,9	21,85								
55	-0,989032	0	16,97	3,34	91,35	9,539	30267,5	0,0653597	227,877	110,913	61057,9	98,9032	3
56	-1,12417	0	17,7333	0,64	91,35	9,4426	34403,1	0,0794232	229,155	167,152	61681	112,417	3
57	-1e+99	24	20,0233	3,34	91,35								
58	-1e+99	0	20,0233	3,34	73,975								
59	-1e+99	30	10,1	10,9	1								
60	-1e+99	8	13,1533	4,42	49,65								
61	-1e+99	2	23,84	3,34	101,775								
62	-0,982939	2	20,0233	3,34	91,35	9,5046	30081	0,0743919	228,252	110,913	61277,6	98,2939	3
63	-1,0092	0	16,97	2,8	84,4	9,5143	30884,8	0,0676761	228,178	119,254	61215,6	100,92	3
64	-0,989821	6	21,55	3,34	91,35	9,5162	30291,6	0,0727771	228,089	114,035	61203,2	98,9821	3
65	-1e+99	0	23,0767	3,34	87,875								
66	-0,978577	0	20,0233	3,34	94,825	9,4946	29947,5	0,0749522	228,387	108,894	61335,7	97,8577	2
67	-1,1887	2	30,71	3,34	21,85	9,2771	36377,9	0,234625	228,842	241,968	62776,5	118,87	3
68	-0,985647	0	17,7333	3,34	94,825	9,5272	30163,9	0,0682878	228,031	110,064	61132,9	98,5647	3
69	-1e+99	0	23,0767	2,8	91,35								
70	-1e+99	14	10,1	4,42	129,575								
71	-1,00195	0	19,26	2,8	98,3	9,4928	30662,9	0,0730599	228,48	117,602	61353,3	100,195	3
72	-0,980486	4	18,4967	3,88	84,4	9,5577	30006	0,0648354	227,54	108,661	60940,2	98,0486	3
73	-1,15777	24	30,71	8,2	21,85	9,4437	35431,4	0,121842	226,874	206,683	61600,5	115,777	3
74	-1,11606	2	31,4733	8,2	21,85	9,3549	34154,8	0,165958	226,976	196,622	62215,8	111,606	3
75	-1e+99	28	20,7867	9,28	67,025								
76	-1e+99	8	13,1533	0,1	136,525								
77	-1e+99	20	20,0233	3,34	94,825								
78	-0,998909	0	20,0233	2,8	80,925	9,4572	30569,8	0,0835637	228,73	119,736	61578,5	99,8909	3
79	-0,995644	18	20,0233	6,58	49,65	9,6787	30469,8	0,0728258	225,951	123,607	60177,5	99,5644	3
80	-0,981396	0	19,26	3,34	94,825	9,5034	30033,8	0,0741146	228,311	109,653	61285,2	98,1396	3
81	-1e+99	0	29,1833	7,66	140								

Figure C.4: Results Sherpa study

Sherpa: Design Table

Design ID	performance	Aft_Arc_Angle	Aft_Ship_Angle	Transom_Angle	Bottom_Radius	Draft	Required_Propeller_	Thrust_deduction_	Shear_resistance	Pressure_resistanc	Wave_Making_Res	PropPowerRatio
82	-1e+99	22	10,1	0,1	140							
83	-0,983633	0	18,4967	3,34	98,3	9,5191	30102,2	0,0720197	228,136	109,524	61184,5	98,3633
84	-0,980159	0	20,0233	3,34	108,725	9,5205	29995,9	0,069278	228,227	106,74	61175,5	98,0159
85	-1e+99	0	13,9167	3,34	94,825							
86	-0,980448	0	20,0233	3,34	112,2	9,5275	30004,8	0,0677234	228,208	106,249	61130,9	98,0448
87	-1e+99	28	29,1833	3,34	1							
88	-0,982363	0	19,26	3,34	98,3	9,5089	30063,4	0,0748608	228,263	109,556	61249,8	98,2363
89	-1e+99	0	26,13	7,66	140							
90	-1e+99	0	10,1	3,88	98,3							
91	-1e+99	30	20,0233	3,34	94,825							
92	-1,02635	0	18,4967	2,26	94,825	9,4816	31409,5	0,0773583	228,696	127,199	61426	102,635
93	-2,11973	24	32,2367	8,2	7,95	9,3779	64870,3	0,21297	225,672	606,915	61815,5	211,973
94	-1,04061	0	15,4433	2,26	80,925	9,5327	31845,8	0,0595711	228,074	129,649	61098	104,061
95	-1e+99	0	23,0767	0,64	4,475	9,296						
96	-0,988701	4	20,0233	3,34	94,825	9,527	30257,3	0,0709816	228,023	112,448	61134,1	98,8701
97	-1e+99	22	26,13	2,8	140							
98	-1e+99	0	26,13	3,34	98,3							
99	-1e+99	24	30,71	8,74	7,95							
100	-1e+99	24	11,6267	3,34	94,825							
101	-1,04117	0	15,4433	2,26	87,875	9,5375	31863	0,0603317	228,053	129,578	61067,4	104,117
102	-1e+99	24	11,6267	8,2	21,85							
103	-1,16146	26	23,0767	2,26	80,925	9,6043	35544,4	0,0647209	226,279	189,091	60642,2	116,146
104	-0,997177	0	15,4433	3,34	94,825	9,5816	30516,7	0,0577896	227,427	111,529	60789,7	99,7177
105	-1e+99	8	33	0,1	140							
106	-0,954037	8	26,8933	6,58	53,125	9,4723	29196,5	0,0973903	227,727	111,207	61476,7	95,4037
107	-0,982009	0	19,26	3,34	84,4	9,4881	30052,5	0,0788193	228,38	111,446	61377,6	98,2009
108	-1e+99	2	24,6033	2,26	108,725							
109	-1,05475	2	15,4433	2,26	80,925	9,5579	32278,6	0,0581214	227,838	133,929	60938,2	105,475
111	-0,962695	18	26,8933	6,58	53,125	9,5314	29461,5	0,0937953	227,051	114,821	61097,1	96,2695
112	-1e+99	18	19,26	9,82	98,3							
113	-0,975661	6	22,3133	3,88	70,5	9,4852	29858,3	0,0802953	228,247	112,315	61396,3	97,5661
114	-1,07731	0	14,68	1,72	87,875	9,5411	32969,1	0,0577183	228,135	142,354	61044,4	107,731
115	-0,958375	4	26,8933	6,58	53,125	9,4594	29329,3	0,0993146	227,976	113,013	61563,4	95,8375
116	-1e+99	0	22,3133	9,82	60,075							
117	-0,959661	6	23,84	4,96	63,55	9,4801	29368,6	0,0909838	228,092	108,717	61429,6	95,9661
118	-1,08511	24	24,6033	8,2	21,85	9,5602	33207,6	0,0721474	225,564	172,775	60874,7	108,511
119	-0,969503	24	30,71	6,58	53,125	9,5143	29669,8	0,0962435	227,131	118,944	61208,9	96,9503
120	-0,956687	8	27,6567	6,58	53,125	9,4637	29277,6	0,102192	227,801	112,684	61534,7	95,6687
121	-1e+99	0	28,42	8,74	112,2							
122	-1e+99	2	27,6567	3,34	84,4							
123	-1e+99	8	23,84	6,58	53,125							
124	-1e+99	8	26,8933	0,64	53,125	9,3418						
125	-0,952071	8	25,3667	6,58	53,125	9,4922	29136,4	0,0972592	227,558	109,47	61347,6	95,2071
126	-1e+99	0	15,4433	6,58	94,825							
128	-1e+99	0	33	0,1	129,575							
129	-1e+99	16	18,4967	9,82	94,825							
130	-1e+99	4	25,3667	6,58	53,125	9,4678	300					0,980292
132	-1e+99	0	15,4433	3,34	101,775							

Figure C.5: Results Sherpa study pt. 2

Bibliography

[1] 2024. URL: https://www.wartsila.com/encyclopedia/term/propeller-clearances.

[2] Jennie Andersson et al. “Propeller–hull interaction beyond the propulsive factors—A case study on the performance of different propeller designs”. In: *Ocean Engineering* 256 (2022), p. 111424. ISSN: 0029-8018. DOI: https://doi.org/10.1016/j.oceaneng.2022.111424. URL: https://www.sciencedirect.com/science/article/pii/S002980182200806X.

[3] Not Available. “SHERPA – An Efficient and Robust Optimization/Search Algorithm”. In: (2019).

[4] Kalyanmoy Deb and Himanshu Jain. “An Evolutionary Many-Objective Optimization Algorithm Using Reference-Point-Based Nondominated Sorting Approach, Part I: Solving Problems With Box Constraints”. In: *Evolutionary Computation, IEEE Transactions on* 18 (Aug. 2014), pp. 577–601. DOI: 10.1109/TEVC.2013.2281535.

[5] Niels Dingemans. *A STUDY ON THE SLOSHING MOTIONS WITHIN A RECTANGULAR MOON-POOL AND THE EFFECT OF IMPLEMENTING APPENDAGES*. 2016.

[6] Sanijo Đurasević et al. “Numerical analysis of self-propulsion flow characteristics in model scale”. In: *Ocean Engineering* 259 (2022), p. 111885. ISSN: 0029-8018. DOI: https://doi.org/10.1016/j.oceaneng.2022.111885. URL: https://www.sciencedirect.com/science/article/pii/S0029801822012252.

[7] L. Eça and M. Hoekstra. “A procedure for the estimation of the numerical uncertainty of CFD calculations based on grid refinement studies”. In: *Journal of Computational Physics* 262 (2014), pp. 104–130. ISSN: 0021-9991. DOI: https://doi.org/10.1016/j.jcp.2014.01.006. URL: https://www.sciencedirect.com/science/article/pii/S0021999114000278.

[8] *Attaining the Asymptotic Range in Rans Simulations*. Vol. ASME 2023 Verification, Validation, and Uncertainty Quantification Symposium. Verification and Validation. May 2023, V001T02A002. DOI: 10.1115/VVUQ2023-108745. eprint: https://asmedigitalcollection.asme.org/VVS/proceedings-pdf/VVUQ2023/86748/V001T02A002/7022885/v001t02a002-vvuq2023-108745.pdf. URL: https://doi.org/10.1115/VVUQ2023-108745.

[9] L. Eça, S.L. Toxopeus, and M. Kerkvliet. “Procedures for the Estimation of Numerical Uncertainties in the Simulation of Steady and Unsteady Flows”. Apr. 2023.

[10] L. Eça et al. “Numerical Errors in Unsteady Flow Simulations”. In: *Journal of Verification, Validation and Uncertainty Quantification* 4.2 (July 2019), p. 021001. ISSN: 2377-2158. DOI: 10.1115/1.4043975. eprint: https://asmedigitalcollection.asme.org/verification/article-pdf/4/2/021001/6412001/vvuq_004_02_021001.pdf. URL: https://doi.org/10.1115/1.4043975.

[11] P. Gallagher et al. “Best Practice Guidelines for the application of Computational Fluid Dynamics in Marine Hydrodynamics”. In: (Apr. 2009). DOI: 10.13140/RG.2.1.4642.7680.

[12] *HEEDS MDO User Guide*. siemens.

[13] J. Holtrop and G.G.J. Mennen. “AN APPROXIMATE POWER PREDICTION METHOD”. In: *International Shipbuilding Progress* (1982).

[14] *ITTC Recommended Procedures and Guidelines*. 2017.

[15] Hrvoje Jasak et al. “CFD validation and grid sensitivity studies of full scale ship self propulsion”. In: *International Journal of Naval Architecture and Ocean Engineering* 11.1 (2019), pp. 33–43. ISSN: 2092-6782. DOI: https://doi.org/10.1016/j.ijnaoe.2017.12.004. URL: https://www.sciencedirect.com/science/article/pii/S2092678217301905.

[16] Marek Kraskowski. “CFD Optimisation of the Longitudinal Volume Distribution of a Ship’s Hull by Constrained Transformation of the Sectional Area Curve”. In: *Polish Maritime Research* 29.3 (2022), pp. 11–20. DOI: doi:10.2478/pomr-2022-0022. URL: https://doi.org/10.2478/pomr-2022-0022.

[17] Auke van der Ploeg, Guus van der Bles, and Jan van Zelderen. “Optimization of a ship with a large diameter propeller”. In: *Numerical Towing Tank Symposium* (2016), pp. 102–107.

[18] Auke van der Ploeg and Bart Schuiling. “Improving an Already Optimized Ship by Making its Stern Asymmetric”. In: *17th Conference on Computer Applications and Information Technology in the Maritime Industries (COMPIT’18), Pavone, Italy* (2018).

[19] Hoyte C. Raven and Joy Klinkenberg. “Practical ship afterbody optimization by multifidelity techniques”. In: *Ship Technology Research* 0.0 (2023), pp. 1–18. DOI: 10.1080/09377255.2023.2275371. eprint: https://doi.org/10.1080/09377255.2023.2275371. URL: https://doi.org/10.1080/09377255.2023.2275371.

[20] Erik Rotteveel, Auke van der Ploeg, and Robert Hekkenberg. “Optimization of ships in shallow water with viscous flow computa-tions and surrogate modeling”. In: *Proceedings of PRADS2016* 4 (2016), 8th.

[21] C. J. Roy and W. L. Oberkampf. “A comprehensive framework for verification, validation, and uncertainty quantification in scientific computing”. In: *Computer Methods in Applied Mechanics and Engineering* 200 (2011), pp. 2131–2144. DOI: https://doi.org/10.1016/j.cma.2011.03.016.

[22] B. Schuiling and T. Terwisga. “Energy Loss Analysis for a Propeller operating behind a Ship”. In: *32nd Symposium on Naval Hydrodynamics* (2018).

[23] B. Schuiling and T. van Terwisga. “Energy Loss Analysis for a Propeller operating behind a Ship”. In: *32nd Symposium on Naval Hydrodynamics Hamburg, Germany* (2018).

[24] Haitham Seada and Kalyan Deb. “Effect of selection operator on NSGA-III in single, multi, and many-objective optimization”. In: May 2015, pp. 2915–2922. DOI: 10.1109/CEC.2015.7257251.

[25] Reza Shamsi, Hassan Ghassemi, and Mehdi Iranmanesh. “A Comparison of the BEM and RANS Calculations for the hydrodynamic performance of the PODS”. In: *Mechanics Industry* 18 (Jan. 2017), p. 205. DOI: 10.1051/meca/2016053.

[26] *Simcenter STAR-CCM+ 2310 User Guide*. siemens.

[27] Hayriye Pehlivan Solak. “Multi-dimensional surrogate based aft form optimization of ships using high fidelity solvers”. In: *Brodogradnja: Teorija i praksa brodogradnje i pomorske tehnike* 71.1 (2020), pp. 85–100.

[28] Yusuke Tahara et al. “Variable decomposition approach applied to multi-objective optimization for minimum powering of commercial ships”. In: *Journal of Marine Science and Technology* 24 (2019), pp. 260–283.

[29] S. Toxopeus. *Numerical Uncertainty Analysis tool*. URL: https://www.marin.nl/en/research/free-resources/verification-and-validation/verification-tools.

[30] Youjiang Wang and Moustafa Abdel-Maksoud. “Coupling wake alignment lifting line method and boundary element method for open water and unsteady propeller simulation”. In: *Ocean Engineering* 213 (2020), p. 107738. ISSN: 0029-8018. DOI: https://doi.org/10.1016/j.oceaneng.2020.107738. URL: https://www.sciencedirect.com/science/article/pii/S0029801820307204.

[31] H.K. Woud and D. Stapersma. *Design of Propulsion and Electric Power Generation Systems*. IMarEST publications. IMarEST, Institute of Marine Engineering, Science and Technology, 2002. ISBN: 9781902536477. URL: https://books.google.nl/books?id=BzRdAAAACAAJ.

[32] Hassan Zakerdoost and Hassan Ghassemi. “Probabilistic surrogate-based optimization of ship hull-propulsor design with bi-level infill sampling technique”. In: *Ocean Engineering* 286 (2023), p. 115614. ISSN: 0029-8018. DOI: https://doi.org/10.1016/j.oceaneng.2023.115614. URL: https://www.sciencedirect.com/science/article/pii/S0029801823019984.

[33] Shenglong Zhang. “Research on the Deep Learning Technology in the Hull Form Optimization Problem”. In: *Journal of Marine Science and Engineering* 10.11 (2022). ISSN: 2077-1312. DOI: 10.3390/jmse10111735. URL: https://www.mdpi.com/2077-1312/10/11/1735.

[34] Cheng Zhao et al. “Optimisation of hull form of ocean-going trawler”. In: *Brodogradnja: Teorija i praksa brodogradnje i pomorske tehnike* 72.4 (2021), pp. 33–46.